

Optimal Spectral Transitions in High-Dimensional Multi-Index Models

Leonardo Defilippis¹, Yatin Dandi^{2,3}, Pierre Mergny², Florent Krzakala², and Bruno Loureiro¹

¹Département d’Informatique, École Normale Supérieure, PSL & CNRS, Paris, France

²Information, Learning, and Physics Laboratory, EPFL, Switzerland

³Sloan School of Management, MIT, United States

Abstract

We consider the problem of how many samples from a Gaussian multi-index model are required to weakly reconstruct the relevant index subspace. Despite its increasing popularity as a testbed for investigating the computational complexity of neural networks, results beyond the single-index setting remain elusive. In this work, we introduce spectral algorithms based on the linearization of a message passing scheme tailored to this problem. Our main contribution is to show that the proposed methods achieve the optimal reconstruction threshold. Leveraging a high-dimensional characterization of the algorithms, we show that above the critical threshold the leading eigenvector correlates with the relevant index subspace, a phenomenon reminiscent of the Baik–Ben Arous–Peche (BBP) transition in spiked models arising in random matrix theory. Supported by numerical experiments and a rigorous theoretical framework, our work bridges critical gaps in the computational limits of weak learnability in multi-index model.

Contents

1	Introduction	2
2	Setting and Notations	4
3	Main Technical Results	7
3.1	Asymmetric spectral method	7
3.2	Symmetric spectral method	9
3.3	Relation between the two spectral methods	11
4	Examples	12
4.1	Asymmetric spectral method	13
4.2	Symmetric spectral method	13
5	Conclusion and Perspectives	14
A	Generalized Approximate Message Passing algorithms	19
A.1	Linear GAMP	19
A.2	State Evolution of Linear GAMP	20

B Derivation of the main results - Asymmetric spectral method	20
C Derivation of the main results - Symmetric spectral method	22
C.1 State Evolution	22
D Details on examples - Asymmetric spectral method	24
D.1 Single-index models	24
D.2 $\text{Cov}[\mathbf{z} y]$ jointly diagonalizable $\forall y$	24
D.2.1 $g(z_1, \dots, z_p) = p^{-1} \sum_{k \in \llbracket p \rrbracket} z_k^2$	26
D.2.2 $g(z_1, z_2) = \text{sign}(z_1 z_2)$	26
D.2.3 $g(z_1, \dots, z_p) = \prod_{k=1}^p z_k$	26
D.3 A non-jointly diagonalizable case: $g(z_1, z_2) = z_1/z_2$	28
E Details on examples - Symmetric spectral method	29
F Proof of Proposition 3.11	30

1 Introduction

A popular model to study learning problems in statistical, computer science and machine learning is the *multi-index model*, where the target function depends on a low-dimensional subspace of the covariates. In this problem, one aim at identifying the p -dimensional linear subspace spanned by a family of orthonormal vectors $\mathbf{w}_{*,1}, \dots, \mathbf{w}_{*,p} \in \mathbb{R}^d$ from n independent observations (\mathbf{x}_i, y_i) from the model:

$$y_i = g(\langle \mathbf{w}_{*,1}, \mathbf{x}_i \rangle, \dots, \langle \mathbf{w}_{*,p}, \mathbf{x}_i \rangle), \quad i \in \llbracket n \rrbracket. \quad (1)$$

This formulation encompasses several fundamental problems in machine learning, signal processing, and theoretical computer science, including: (i) Linear estimation, where $p = 1$ and $g(z) = z$, (ii) Phase retrieval, where $p = 1$ and $g(z) = |z|$. (iii) Learning Two-layer neural networks, where p is the width and $g(\mathbf{z}) = \sum_{j \in \llbracket p \rrbracket} a_j \sigma(z_j)$ for some non-linear activation function $\sigma : \mathbb{R} \rightarrow \mathbb{R}$, or (iv) learning Sparse parity functions, where $g(\mathbf{z}) = \text{sign}(\prod_{j \in \llbracket p \rrbracket} z_j)$.

A classical problem in statistics [Friedman and Stuetzle \[1981\]](#), [Yuan \[2011\]](#), [Babichev and Bach \[2018\]](#), the multi-index model has recently gained in popularity in the machine learning community as a generative model for supervised learning data where the labels only depend on an underlying low-dimensional latent subspace of the covariates [Aubin et al. \[2018\]](#), [Damian et al. \[2022\]](#), [Dandi et al. \[2024a\]](#).

Of particular interest to this work are spectral methods, which play a fundamental role in machine learning by offering an efficient and computationally tractable approach to extracting meaningful structure from high-dimensional noisy data. A paradigmatic example is the Baik–Ben Arous–Péché (BBP) transition [Baik et al. \[2005\]](#), where the leading eigenvalue of a matrix correlates with the hidden signal — a phenomenon that is ubiquitous in machine learning theory. Beyond their practical utility, spectral methods often serve as a starting point for more advanced approaches, including iterative and nonlinear techniques. This leads us to the central question of this paper:

Can one design optimal spectral methods that minimizes the amount of data required for identifying the hidden subspace in multi-index models?

While the optimal spectral method for single-index models are well understood [Luo et al. \[2019\]](#), [Mondelli and Montanari \[2018\]](#), [Maillard et al. \[2022\]](#), [Mondelli et al. \[2022\]](#), and their optimality in terms of weak recovery threshold established [Barbier et al. \[2019\]](#), [Mondelli and Montanari \[2018\]](#) their counterparts for multi-index models remain largely unexplored. This gap is particularly important, as multi-index models serve as a natural testbed for studying the computational complexity of feature learning in modern machine learning, and have attracted much attention recently [Abbe et al. \[2023\]](#), [Damian et al. \[2022\]](#), [Dandi et al. \[2024a\]](#), [Arnaboldi et al. \[2023\]](#), [Collins-Woodfin et al. \[2024\]](#), [Berthier et al. \[2024\]](#), [Simsek et al. \[2024\]](#).

Main contributions — In this work, we step up to this challenge by constructing optimal spectral methods for multi-index models. We introduce and analyze spectral algorithms based on a linearized message-passing framework, specifically tailored to this setting. Our main contribution is to present two such constructions, establish the reconstruction threshold for these methods and to show that they achieve the provably optimal threshold for weak recovery among efficient algorithms [Troiani et al. \[2024\]](#).

Other Related works –

- Recently, multi-index models have become a proxy model for studying non-convex optimization [Veiga et al. \[2022\]](#), [Arnaboldi et al. \[2023\]](#), [Collins-Woodfin et al. \[2024\]](#). [Arous et al. \[2021\]](#) has shown that the sample complexity of one-pass SGD for single-index model is governed by the *information exponent* of the link function. This analysis was generalized in several directions, such as to other architectures [Berthier et al. \[2024\]](#), larger batch sizes [Arnaboldi et al. \[2024a\]](#) and to overparametrised models [Arnaboldi et al. \[2024c\]](#). A similar notion, known as the *leap exponent*, was introduced for multi-index models, where it was shown that different index subspaces might be learned hierarchically according to their interaction [Abbe et al. \[2022, 2023\]](#), [Bietti et al. \[2023\]](#), [Mousavi-Hosseini et al. \[2024\]](#). The picture was found to be different for batch algorithms exploiting correlations in the data [Dandi et al. \[2024b\]](#), [Arnaboldi et al. \[2024b\]](#), [Lee et al. \[2024\]](#), achieving a sample complexity closer to optimal first order methods [Barbier et al. \[2019\]](#), [Damian et al. \[2024\]](#), [Troiani et al. \[2024\]](#). [Troiani et al. \[2024\]](#) in particular, provided optimal asymptotic thresholds for weak recovery within the class of first order methods.
- Spectral methods are widely employed as a warm start strategy for initializing other algorithms, in particular for iterative schemes (such as gradient descent) for which random initialization is a fixed point. Relevant to this work is the class of approximate message passing (AMP) algorithms, which have garnered significant interest in the high-dimensional statistics and machine learning communities over the past decade [Donoho et al. \[2009\]](#), [Bayati and Montanari \[2011\]](#), [Rangan \[2011\]](#), [Fletcher and Rangan \[2018\]](#). AMP for multi-index models was discussed in [Aubin et al. \[2018\]](#), [Troiani et al. \[2024\]](#). Spectral initialization for AMP in the context of single-index models has been studied by [Mondelli and Venkataramanan \[2021\]](#).
- The interplay between AMP and spectral methods has been extensively studied in the literature, see for example [Saade et al. \[2014\]](#), [Lesieur et al. \[2017\]](#), [Aubin et al. \[2019\]](#), [Mondelli and Montanari \[2018\]](#), [Mondelli et al. \[2022\]](#), [Maillard et al. \[2022\]](#), [Venkataramanan et al. \[2022\]](#). In particular the idea of using message passing algorithm to derive spectral method has been very successful, leading to the non-backtracking matrix [Krzakala et al. \[2013\]](#) and more recently to the Kikuchi hierarchy [Wein et al. \[2019\]](#), [Hsieh et al. \[2023\]](#), and to non-linear optimal spectral methods for matrix and tensor factorization [Lesieur et al. \[2017\]](#), [Perry et al. \[2018\]](#), [Guionnet et al. \[2023\]](#), [Pak et al. \[2024\]](#).

2 Setting and Notations

Notations — To enhance readability, we adopt the following consistent notations through the paper: scalar quantities are denoted using non-bold font (e.g., a or A), vectors are represented in bold lowercase letters (e.g., \mathbf{a}), matrices are written in bold uppercase letters (e.g., \mathbf{A}), and tensors are depicted using underlined bold uppercase letters (e.g., $\underline{\mathbf{A}}$). We further differentiate random variables depending on the noise with non-italic font (e.g., $a, \mathbf{a}, \mathbf{A}, \underline{\mathbf{A}}$). We denote by $\langle \mathbf{a}, \mathbf{b} \rangle$ the standard Euclidean scalar product, $\|\mathbf{a}\|$ the ℓ^2 -norm of a vector \mathbf{a} , $\|\mathbf{A}\|_{\text{op}}$ the operator norm of a matrix \mathbf{A} and $\|\mathbf{A}\|_{\text{F}}$ its Frobenius norm. Given $n \in \mathbb{N}$, we use the shorthand $\llbracket n \rrbracket = \{1, \dots, n\}$. We denote \mathbb{S}_+^p the cone of positive semi-definite $p \times p$ matrices. $(x)_+ := \max(0, x)$.

The Gaussian Multi Index Model — We consider the supervised learning setting with n i.i.d. samples $(\mathbf{x}_i, y_i)_{i \in \llbracket n \rrbracket}$ with covariates $\mathbf{x}_i \sim \mathcal{N}(\mathbf{0}, d^{-1} \mathbf{I}_d) \in \mathbb{R}^d$ and labels y drawn conditionally from the Gaussian *multi-index model* defined by

$$y \sim \mathbb{P}(\cdot | \mathbf{W}_\star^T \mathbf{x}) = \mathbb{P}\left(\cdot \mid \begin{bmatrix} \langle \mathbf{w}_{\star,1}, \mathbf{x} \rangle \\ \vdots \\ \langle \mathbf{w}_{\star,p}, \mathbf{x} \rangle \end{bmatrix}\right), \quad (2)$$

where $\mathbf{W}_\star := (\mathbf{w}_{\star,1}, \dots, \mathbf{w}_{\star,p}) \in \mathbb{R}^{d \times p}$ is a weight matrix with independant columns with $\mathbf{w}_{\star,j} \sim \mathcal{N}(\mathbf{0}, \mathbf{I}_d)$, $j \in \llbracket p \rrbracket$ and $\mathbb{P}(\cdot | \cdot)$ is a conditional probability distribution. Additionally, we define the *link function* $g : \mathbb{R}^p \ni \mathbf{z} \mapsto g(\mathbf{z}) \in \mathbb{R}$ as the conditional mean

$$g(\mathbf{z}) := \mathbb{E}\{y | \mathbf{W}_\star^T \mathbf{x} = \mathbf{z}\} = \int y \, d\mathbb{P}(y | \mathbf{z}), \quad (3)$$

and the labels' marginal distribution

$$Z(y) = \mathbb{E}_{\mathbf{W}_\star} \mathbb{E}_{\mathbf{x} \sim \mathcal{N}(\mathbf{0}, d^{-1} \mathbf{I}_d)} [\mathbb{P}(y | \mathbf{W}_\star^T \mathbf{x})]. \quad (4)$$

Note that, in the limit $d \rightarrow \infty$, for $\mathbf{x} \sim \mathcal{N}(\mathbf{0}, d^{-1} \mathbf{I})$, the Central Limit Theorem implies $\mathbf{W}_\star^T \mathbf{x} \sim \mathcal{N}(\mathbf{0}, \mathbf{I}_p)$ and $Z(y) = \mathbb{E}_{\mathbf{z} \sim \mathcal{N}(\mathbf{0}, \mathbf{I}_p)} [\mathbb{P}(y | \mathbf{z})]$.

We investigate the problem of reconstructing \mathbf{W}_\star in the proportional *high-dimensional* limit

$$d, n \equiv n(d) \rightarrow \infty \quad \text{such that} \quad n/d \rightarrow \alpha \in \mathbb{R}_+. \quad (5)$$

In particular we are interested in the existence of an estimator $\hat{\mathbf{W}}$ that correlates with the weight matrix \mathbf{W}_\star better than a random estimator. This is formalized as follows.

Definition 2.1. (Weak subspace recovery) Given an estimator $\hat{\mathbf{W}}$ of \mathbf{W}_\star with $\|\hat{\mathbf{W}}\|_{\text{F}} = \Theta(d)$, we say we have *weak recovery* of a subspace $V \subset \mathbb{R}^d$, if

$$\inf_{\mathbf{v} \in V \cap \mathbb{S}^{d-1}} \|\hat{\mathbf{W}}^T \mathbf{W}_\star \mathbf{v}\| = \Theta(1), \quad (6)$$

with high probability.

Computational bottlenecks for weak recovery in the Gaussian multi-index models have been studied by [Troiani et al. \[2024\]](#) using an optimal *generalized approximate message passing* (GAMP) scheme, see Appendix A for a detailed discussion of the algorithm. In particular, for the appropriate choice of denoiser functions, given in eq. (58), AMP is provably optimal among first-order methods

Celentano et al. [2020], Montanari and Wu [2024]. Their work provides a classification of the directions in \mathbb{R}^p in terms of computational complexity of their weak learnability. In particular, if and only if

$$\mathbb{E}_{\mathbf{z} \sim \mathbf{N}(\mathbf{0}, \mathbf{I}_p)}[\mathbf{z} \mathbf{P}(\mathbf{y}|\mathbf{z})] \propto \mathbb{E}[\mathbf{z}|\mathbf{y}] = \mathbf{0} \quad (7)$$

almost surely over $\mathbf{y} \sim \mathbf{Z}$, the subspace of directions that can be learned in a finite number of iterations is empty, for AMP randomly initialized. Nonetheless, if the initialization contains an arbitrarily small (but finite) amount of *side-information* about the ground truth weights \mathbf{W}_* , AMP can weakly recover a subspace of \mathbb{R}^p , provided that $\alpha > \alpha_c$, where the critical sample complexity is characterized in Lemma 2.2.

Lemma 2.2. *Troiani et al. [2024], Stability of the uninformed fixed point and critical sample complexity] If $\mathbf{M} = \mathbf{0} \in \mathbb{R}^{p \times p}$ is a fixed point of the state evolution associated to the optimal GAMP (58), then it is an unstable fixed point if and only if $\|\mathcal{F}(\mathbf{M})\|_F > 0$ and $n > \alpha_c d$, where the critical sample complexity α_c is:*

$$\alpha_c^{-1} = \sup_{\mathbf{M} \in \mathbb{S}_p^+, \|\mathbf{M}\|_F=1} \|\mathcal{F}(\mathbf{M})\|_F, \quad (8)$$

with

$$\mathcal{F}(\mathbf{M}) := \mathbb{E}_{\mathbf{y} \sim \mathbf{Z}} [(\mathbf{Cov}[\mathbf{z}|\mathbf{y}] - \mathbf{I}) \mathbf{M} (\mathbf{Cov}[\mathbf{z}|\mathbf{y}] - \mathbf{I})^T], \quad (9)$$

Moreover, if $\|\mathcal{F}(\mathbf{M})\|_F = 0$, then $\mathbf{M} = \mathbf{0}$ is a stable fixed point for any $n = \Theta(d)$.

The aim of our work is to close this gap, providing an estimation procedure that achieves weak recovery at the same critical threshold α_c defined in eq. (8), but crucially *does not require an informed initialization*.

In what follows we restrict the problem defined in (3) to the set of link functions satisfying eq. (7). These functions (said to have a *generative exponent* 2 in the terminology of Damian et al. [2024]) covers a large class of the relevant problems, with the exception of the really hard functions such as sparse parities, which cannot be solved efficiently with a linear (in d number of samples Troiani et al. [2024]).

Throughout this manuscript, we adopt the following definitions for tensor operations and tensor eigenpairs.

Definition 2.3. (Tensor Contraction) For a tensor of order 4 of the form $\underline{\mathbf{A}} = (A_{ijkl}) \in \mathbb{R}^{\nu \times p \times \nu \times p}$ with $\nu = n$ or $\nu = d$, we define the contraction of such tensor with a matrix $\mathbf{B} \in \mathbb{C}^{\nu \times p}$ by the operation $\underline{\mathbf{A}} \cdot \mathbf{B} \in \mathbb{R}^{d \times p}$ such that

$$(\underline{\mathbf{A}} \cdot \mathbf{B})_{kh} := \sum_{i \in [\nu]} \sum_{j \in [p]} A_{ijkl} B_{ij} \quad k \in [\nu], h \in [p]. \quad (10)$$

The tensor $\underline{\mathbf{A}}$ is symmetric if $\langle \underline{\mathbf{A}} \cdot \mathbf{B}, \mathbf{C} \rangle = \langle \mathbf{B}, \underline{\mathbf{A}} \cdot \mathbf{C} \rangle$ (equivalently $A_{ijkl} = A_{jikl}$ and $A_{ijkl} = A_{ijhk}$, for all $i, j \in [\nu]$, $k, h \in [p]$).

Definition 2.4. (Tensor Inversion) A tensor $\underline{\mathbf{A}}$ is *invertible* if and only if there exists a tensor $\underline{\mathbf{A}}^{-1} \in \mathbb{R}^{\nu \times p \times \nu \times p}$ such that,

$$\underline{\mathbf{A}}^{-1} \cdot (\underline{\mathbf{A}} \cdot \mathbf{B}) = \underline{\mathbf{A}} \cdot (\underline{\mathbf{A}}^{-1} \cdot \mathbf{B}) = \underline{\mathbf{I}} \mathbf{B} = \mathbf{B} \quad (11)$$

holds for all $\mathbf{B} \in \mathbb{R}^{\nu \times p}$ and where $\underline{\mathbf{I}} = (I_{ijkl})$ is the identity tensor, $I_{ijkl} := \delta_{ij} \delta_{kh}$.

In this framework, $\underline{\mathbf{A}}$ acts as a linear operator in the vector space of $\nu \times p$ matrices, with inner product $\langle \mathbf{B}, \mathbf{C} \rangle := \text{Tr}(\mathbf{B}^T \mathbf{C})$ leading to the following natural definition of eigenpairs.

Definition 2.5. (Tensor Eigenpairs) We say that $(\lambda, \mathbf{V}) \in \mathbb{C} \times \mathbb{R}^{\nu \times p} \setminus \{\mathbf{0}_{\nu \times p}\}$ is an *eigenpair* of a tensor $\underline{\mathbf{A}} \in \mathbb{R}^{\nu \times p \times \nu \times p}$ if the following equation holds

$$\underline{\mathbf{A}} \cdot \mathbf{V} = \lambda \mathbf{V}. \quad (12)$$

For the spectral theorem, a symmetric tensor admit an orthonormal basis of eigenvectors in $\mathbb{R}^{\nu \times p}$, corresponding to real eigenvalues.

Remark 2.6. (Flattened Tensor) One can equivalently consider a *flatten* version of tensor, that is the matrix $\mathbf{flat}(\underline{\mathbf{A}}) \in \mathbb{R}^{\nu p \times \nu p}$ such that

$$\begin{aligned} (\mathbf{flat}(\underline{\mathbf{A}}))_{uv} &:= A_{ijkh} \\ u &= (i-1)p + j, \quad v = (k-1)p + h. \end{aligned} \quad (13)$$

Similarly a *flatten* version of a matrix is defined as $\mathbf{flat}(\mathbf{V}) \in \mathbb{R}^{\nu p}$ such that $(\mathbf{flat}(\mathbf{V}))_u = V_{ij}$ with $u = (i-1)p + j$. A classical eigenpair of $\mathbf{flat}(\underline{\mathbf{A}})$ is then related to the former definition 2.5 of the tensor eigenpair by $(\lambda, \mathbf{flat}(\mathbf{V}))$. By abuse of notation, we will write $\|\underline{\mathbf{T}}\|_{\text{op}} = \|\mathbf{flat}(\underline{\mathbf{T}})\|_{\text{op}}$.

We can now introduce the Spectral Methods we aim to investigate. Given a matrix $\mathbf{X} \in \mathbb{R}^{n \times d}$ with rows $\mathbf{x}_i \sim \mathcal{N}(\mathbf{0}, d^{-1} \mathbf{I}_d)$ and a vector of labels $\mathbf{y} \in \mathbb{R}^n$ with elements sampled as in (3), define the tensor $\underline{\mathbf{G}} \in \mathbb{R}^{n \times p \times n \times p}$, acting on $n \times p$ matrices as described in Definition 2.5, as

$$G_{ikjh} = \delta_{ij} \mathbb{E}[\mathbf{z}_k \mathbf{z}_h | y_i] - \delta_{ij} \delta_{kh}, \quad i, j \in \llbracket n \rrbracket, k, h \in \llbracket p \rrbracket. \quad (14)$$

where δ_{ij} is the Kronecker delta.

Given these definitions, define the following two spectral estimators $\hat{\mathbf{W}}_{\underline{\mathbf{L}}}, \hat{\mathbf{W}}_{\underline{\mathbf{T}}}$ of the weight matrix \mathbf{W}_* as

1. Asymmetric spectral method:

$$\hat{\mathbf{W}}_{\underline{\mathbf{L}}} := \sqrt{dN} \frac{\mathbf{X}^T \underline{\mathbf{G}} \cdot \underline{\boldsymbol{\Omega}}_1}{\|\mathbf{X}^T \underline{\mathbf{G}} \cdot \underline{\boldsymbol{\Omega}}_1\|_{\text{F}}}, \quad (15)$$

where $\underline{\boldsymbol{\Omega}}_1$ is the (matrix) eigenvector corresponding to the eigenvalue $\gamma_1^{\underline{\mathbf{L}}}$ with largest real part of the tensor $\underline{\mathbf{L}} \in \mathbb{R}^{n \times p \times d \times p}$ defined for any $\underline{\boldsymbol{\Omega}} \in \mathbb{R}^{n \times p}$ by:

$$\underline{\mathbf{L}} \cdot \underline{\boldsymbol{\Omega}} := (\mathbf{X} \mathbf{X}^T - \mathbf{I}_n) \underline{\mathbf{G}} \cdot \underline{\boldsymbol{\Omega}}. \quad (16)$$

Note that the constant N can be chosen to fix the normalization of $d^{-1} \|\hat{\mathbf{W}}\|_{\text{F}}^2 = N$.

2. Symmetric spectral method:

$$\hat{\mathbf{W}}_{\underline{\mathbf{T}}} := \sqrt{dN} \frac{\mathbf{W}_1}{\|\mathbf{W}_1\|_{\text{F}}}, \quad (17)$$

where \mathbf{W}_1 is the (matrix) eigenvector associated to the largest eigenvalue $\gamma_1^{\underline{\mathbf{T}}}$ of the symmetric tensor map $\underline{\mathbf{T}} \in \mathbb{R}^{d \times p \times d \times p}$ defined as

$$\underline{\mathbf{T}} \cdot \mathbf{W} := \mathbf{X}^T \underline{\mathbf{G}} \cdot ((\underline{\mathbf{G}} + \underline{\mathbf{I}})^{-1} \cdot (\mathbf{X} \mathbf{W})) \quad (18)$$

Note that the constant N is arbitrary and can be chosen to fix $d^{-1} \|\hat{\mathbf{W}}_{\underline{\mathbf{L}}}\|_{\text{F}}^2 = d^{-1} \|\hat{\mathbf{W}}_{\underline{\mathbf{T}}}\|_{\text{F}}^2 = N$.

At first glance, these two spectral estimators may appear ad hoc or lacking a clear theoretical justification. However, they can be motivated by a linearization of the optimal GAMP algorithm around the non-informative fixed point:

$$\delta\Omega^t = \mathbf{X} \delta\hat{\mathbf{W}}^t - \underline{\mathbf{G}} \cdot \delta\Omega^{t-1}, \quad (19)$$

$$\delta\hat{\mathbf{W}}^{t+1} = \mathbf{X}^T \underline{\mathbf{G}} \cdot \delta\Omega^t. \quad (20)$$

Substituting eq. (20) into eq. (20), this is equivalent to $\delta\Omega^{t+1} = \underline{\mathbf{L}} \cdot \delta\Omega^t$. Moreover, assuming convergence,¹ one ends up with

$$\delta\Omega = \underline{\mathbf{L}} \cdot \delta\Omega \quad (21)$$

$$\delta\hat{\mathbf{W}} = \underline{\mathbf{T}} \cdot \delta\hat{\mathbf{W}}. \quad (22)$$

This suggests that at first leading order in the estimates, the dynamics is governed by power-iteration (and respectively a variant of it) on the tensor $\underline{\mathbf{L}}$ (respectively the symmetric tensor $\underline{\mathbf{T}}$) defined previously. As power iteration converges under mild assumptions to the top (matrix) eigenvector of the tensor, this further suggests to use the top eigenvectors $\hat{\mathbf{W}}_{\underline{\mathbf{L}}}, \hat{\mathbf{W}}_{\underline{\mathbf{T}}}$ of the corresponding tensors as an estimate for the weight matrix \mathbf{W}_* .

Additional details on the linearized GAMP are reported in Appendix A.1. Similar approaches have been thoroughly investigated in the context of single-index models [Mondelli and Montanari \[2018\]](#), [Maillard et al. \[2022\]](#), community detection [Krzakala et al. \[2013\]](#), [Saade et al. \[2014\]](#), spiked matrix estimation [Lesieur et al. \[2017\]](#), [Aubin et al. \[2019\]](#), where they have been provably shown to provide a non-vanishing correlation with the ground truth exactly at the optimal weak recovery threshold. It is interesting to notice that the spectral estimators $\hat{\mathbf{W}}_{\underline{\mathbf{L}}}$ and $\hat{\mathbf{W}}_{\underline{\mathbf{T}}}$ correspond to the generalization for multi-index models of the spectral methods derived in [Maillard et al. \[2022\]](#), respectively from the linearization of the optimal Vector Approximate Message Passing [Schniter et al. \[2016\]](#), [Rangan et al. \[2017\]](#) and the Hessian of the TAP free energy associated to the posterior distribution for the weights [Saade et al. \[2014\]](#). In particular, for $p=1$, the matrices proposed in our manuscript exactly reduce to the two ones (called respectively "TAP" and "LAMP") investigated in [Maillard et al. \[2022\]](#).

3 Main Technical Results

In order to characterize the weak recovery of the proposed spectral methods, we define two message passing schemes tailored to respectively have eigenvectors of $\underline{\mathbf{L}}$ and $\underline{\mathbf{T}}$ as fixed points. Similarly to these previous works, we leverage the *state evolution* associated to the algorithms in order to quantify the alignment between the spectral estimators and the weight matrix \mathbf{W}_* , tracking the overlap matrices

$$\mathbf{M}^t := \frac{1}{d} \left(\hat{\mathbf{W}}^t \right)^T \mathbf{W}_*, \quad \mathbf{Q}^t := \frac{1}{d} \left(\hat{\mathbf{W}}^t \right)^T \hat{\mathbf{W}}^t, \quad (23)$$

and their value \mathbf{M}, \mathbf{Q} , at convergence. The state evolution equations for generic linear GAMP algorithms are presented in Appendix A.2.

3.1 Asymmetric spectral method

Definition 3.1. Consider the linear GAMP algorithm (55,56) with denoiser functions

$$\mathbf{g}_{\text{out}}^t(\omega, y) = \mathbf{G}(y)\omega := (\text{Cov}[\mathbf{z}|y] - \mathbf{I})\omega, \quad \mathbf{f}_{\text{in}}^t(\mathbf{b}) = \gamma^{-1}\mathbf{b}, \quad (24)$$

¹Here and in the rest of the paper, we drop the time index t to refer to the quantities at convergence.

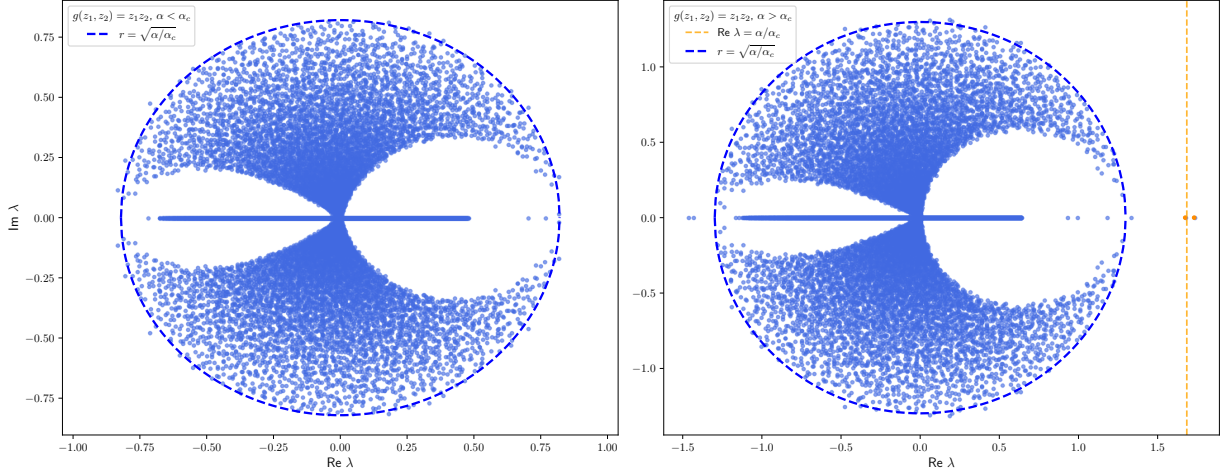


Figure 1: Distribution of the eigenvalues (dots) $\lambda \in \mathbb{C}$ of $\underline{\mathbf{L}}$ at finite $n = 10^4$, for $g(z_1, z_2) = z_1 z_2$, $\alpha_c \approx 0.59375$. **(Left)** $\alpha = 0.4 < \alpha_c$. **(Right)** $\alpha = 1 > \alpha_c$. The dashed blue circle has radius equal to $\sqrt{\alpha/\alpha_c}$, i.e. the value γ_b predicted in Lemma 3.4. The dashed orange vertical line corresponds to $\text{Re } \lambda = \alpha/\alpha_c$, the eigenvalue γ_s defined in Lemma 3.3. As predicted by the state evolution equations for this problem, two significant eigenvalues (highlighted in orange) are observed near this vertical line.

with $\gamma > 0$ a parameter to be fixed. Its iterations read

$$\Omega^t = \mathbf{X} \hat{\mathbf{W}}^t - \gamma^{-1} \underline{\mathbf{G}} \cdot \Omega^{t-1}, \quad (25)$$

$$\hat{\mathbf{W}}^{t+1} = \gamma^{-1} \mathbf{X}^T \underline{\mathbf{G}} \cdot \Omega^t, \quad (26)$$

When γ is chosen as an eigenvalue of $\underline{\mathbf{L}}$, the correspondent eigenvector is a fixed point of eq. (25). In the high-dimensional limit, the asymptotic overlap of the estimator $\hat{\mathbf{W}}$ in (26) can be tracked thanks to the state evolution equations, which follow from an immediate application of the general result of [Javanmard and Montanari \[2013\]](#) to the GAMP algorithm (3.6).

Proposition 3.2 (State evolution [Javanmard and Montanari \[2013\]](#)). *Let \mathbf{M}^t and \mathbf{Q}^t denote the overlaps defined in eq. (23) for the iterative algorithm (3.1). Then, in the proportional high-dimensional limit $n, d \rightarrow \infty$ at fixed $\alpha = n/d$, they satisfy the following state evolution:*

$$\mathbf{M}^{t+1} = \alpha \gamma^{-1} \mathcal{F}(\mathbf{M}^t) \quad (27)$$

$$\mathbf{Q}^{t+1} = \mathbf{M}^t (\mathbf{M}^t)^T + \alpha \gamma^{-2} (\mathcal{G}(\mathbf{M}^t) + \mathcal{F}(\mathbf{Q}^t)) \quad (28)$$

where

$$\mathcal{F}(\mathbf{M}) := \mathbb{E}_y [\mathbf{G}(y) \mathbf{M} \mathbf{G}(y)], \quad (29)$$

$$\mathcal{G}(\mathbf{M}) := \mathbb{E}_y [\mathbf{G}(y) \mathbf{M} \mathbf{G}(y) \mathbf{M}^T \mathbf{G}(y)]. \quad (30)$$

With the state evolution equations in hand, one can derive a sharp characterization of the asymptotic weak recovery threshold in terms of the spectral properties of the estimator by a linear stability argument [Strogatz \[2001\]](#)

Lemma 3.3. For $\alpha > \alpha_c$, $\gamma_s = \alpha/\alpha_c$ is the largest value of γ such that the state evolution 3.2 has a stable fixed point (\mathbf{M}, \mathbf{Q}) with

$$\mathbf{M} \neq \mathbf{0}, \quad \mathbf{Q} \in \mathbb{S}_+^p \setminus \{\mathbf{0}\}. \quad (31)$$

Additionally, $\mathbf{M} \in \mathbb{S}_+^p \setminus \{\mathbf{0}\}$.

Lemma 3.4. For all $\alpha \in \mathbb{R}$, $\gamma_b = \sqrt{\alpha/\alpha_c}$ is the largest value for γ such that the state evolution 3.2 has a fixed point (\mathbf{M}, \mathbf{Q}) with

$$\mathbf{M} = \mathbf{0}, \quad \mathbf{Q} \in \mathbb{S}_+^p \setminus \{\mathbf{0}\}. \quad (32)$$

The fixed point is stable for $\alpha < \alpha_c$ and unstable otherwise.

The derivation of the Lemmas is outlined in Appendix B. This two results indicate a change of behavior of the operator norm of $\underline{\mathbf{L}}$ at the critical value α_c , leading to the following conjecture.

Conjecture 3.5. In the high-dimensional limit $n, d \rightarrow \infty$, $n/d \rightarrow \alpha$, the empirical spectral distribution associated to the pn eigenvalues of $\underline{\mathbf{L}}$ converges weakly almost surely to a density whose support is strictly contained in a disk of radius $\gamma_b = \sqrt{\alpha/\alpha_c}$ centered at the origin. Moreover

- for $\alpha < \alpha_c$, $\|\underline{\mathbf{L}}\|_{\text{op}} \xrightarrow[n \rightarrow \infty]{a.s.} \gamma_b$ and the associated eigenvector is not correlated with \mathbf{W}_\star ;
- for $\alpha > \alpha_c$, $\|\underline{\mathbf{L}}\|_{\text{op}} \xrightarrow[n \rightarrow \infty]{a.s.} \gamma_s > \gamma_b$ and the associated eigenvector defined in (16), weakly recovers the signal.

This conjecture, motivated by the results (3.3-3.4) is perfectly supported by extensive simulations, as illustrated in Fig. 1, 2. A rigorous proof requires, however, a finer control of the spectral norm of these operators.

3.2 Symmetric spectral method

In order to simplify the notation, define the symmetric $p \times p$ matrix

$$\mathcal{T}(y) := \mathbf{I} - \text{Cov}^{-1}[\mathbf{z}|y]. \quad (33)$$

Definition 3.6. Consider the linear GAMP algorithm (55,56) with denoiser functions

$$\mathbf{g}_{\text{out}}^t(\boldsymbol{\omega}, y) = \mathcal{T}(y) \mathbf{V}_t (a_t \mathbf{I} - \mathbf{V}_t \mathcal{T}(y) \mathbf{V}_t)^{-1} \boldsymbol{\omega}, \quad (34)$$

$$\mathbf{f}_{\text{in}}^{t+1}(\mathbf{b}) = \mathbf{V}_{t+1} \mathbf{b}, \quad (35)$$

with

$$\mathbf{V}_{t+1} = \left(\gamma_t \mathbf{V}_t - \alpha \mathbb{E}_{y \sim \mathbf{Z}} \left[\mathcal{T}(y) \mathbf{V}_t (a_t \mathbf{I} - \mathbf{V}_t \mathcal{T}(y) \mathbf{V}_t)^{-1} \right] \right)^{-1}, \quad (36)$$

a_t a parameter to be fixed and γ_t chosen, a posteriori, such that $\|\mathbf{V}_{t+1}\|_{\text{op}} = 1$. Note that \mathbf{V}_t is symmetric at all times given a symmetric initialization \mathbf{V}_0 .

In Appendix C we show that, for properly chosen a_t , the fixed point for the iterate $\hat{\mathbf{W}}^t \mathbf{V}_t$ is the eigenvector of $\underline{\mathbf{T}}$ with eigenvalue $\lim_{t \rightarrow \infty} a_t \gamma_t$. The denoiser functions chosen for this GAMP algorithm are derived as a generalization of the ones in Zhang et al. [2024], where a similar approach has been used to characterize the recovery properties of spectral algorithms for structured single-index models.

Proposition 3.7 (State evolution Javanmard and Montanari [2013], Mondelli and Montanari [2018]). *Let \mathbf{M}^t and \mathbf{Q}^t denote the overlaps defined in eq. (23) for the iterative algorithm (3.6). Then, in the proportional high-dimensional limit $n, d \rightarrow \infty$ at fixed $\alpha = n/d$, they satisfy the following state evolution equations:*

$$\begin{aligned}\mathbf{M}^{t+1} &= \alpha \mathcal{F}(\mathbf{M}^t; a_t, \mathbf{V}_t), \\ \mathbf{Q}^{t+1} &= \mathbf{M}^t (\mathbf{M}^t)^T + \alpha (\mathcal{G}(\mathbf{M}^t; a_t, \mathbf{V}_t) + \tilde{\mathcal{F}}(\mathbf{Q}^t; a_t, \mathbf{V}_t)),\end{aligned}\tag{37}$$

where we have defined the symmetric operator

$$\mathcal{F}(\mathbf{M}; a_t, \mathbf{V}_t) := \mathbb{E}_{y \sim \mathbf{Z}} \left[\mathbf{V}_t \mathcal{T}(y) \mathbf{V}_t (a_t - \mathbf{V}_t \mathcal{T}(y) \mathbf{V}_t)^{-1} \mathbf{M} (\text{Cov}[\mathbf{z}|y] - \mathbf{I}) \right], \tag{38}$$

while $\tilde{\mathcal{F}}$ and \mathcal{G} are given in eq. (97,98).

The complete set of state evolutions equation is displayed in Appendix C.1. For $a = 1$, the fixed point for eq. (36) is $\mathbf{V} = \mathbf{I}$ and the operators $\mathcal{F}(\mathbf{M}; 1, \mathbf{I})$ and $\tilde{\mathcal{F}}(\mathbf{M}; 1, \mathbf{I})$ coincide with $\mathcal{F}(\mathbf{M})$ defined in (9), having the largest eigenvalue correspondent to α_c^{-1} . As $a \rightarrow \infty$, $\mathbf{V} \rightarrow \mathbf{I}$ and $\mathcal{F}(\cdot; a, \mathbf{V}(a)) \rightarrow \mathbf{0}$. Therefore, since the operator depends continuously on $a \in [1, \infty)$, there exists a continuous function $\nu_1^{\mathcal{F}}(a)$ for the largest eigenvalue of the operator as a function of the parameter a , with $\nu_1^{\mathcal{F}}(1) = \alpha_c^{-1}$ and $\nu_1^{\mathcal{F}}(a \rightarrow \infty) \rightarrow 0$. Hence, for all $\alpha > \alpha_c$, there exists $a > 1$ such that $\nu_1^{\mathcal{F}}(a) = \alpha^{-1}$. A similar argument applies to $\tilde{\mathcal{F}}$ and its largest eigenvalue $\nu_1^{\tilde{\mathcal{F}}}(a)$.

Lemma 3.8. *For $\alpha > \alpha_c$, consider $a_t = a > 1$ solution of $\nu_1^{\mathcal{F}}(a_t) = \alpha^{-1}$ and γ_t such that $\|\mathbf{V}_{t+1}\|_{\text{op}} = 1$, with \mathbf{V}_{t+1} given by eq. (36). Then, the state evolution has a stable fixed point (\mathbf{M}, \mathbf{Q}) with*

$$\mathbf{M} \neq \mathbf{0}, \quad \mathbf{Q} \in \mathbb{S}_+^p \setminus \{\mathbf{0}\}, \tag{39}$$

correspondent to the eigenvalue $\lambda_s = a\gamma$.

Lemma 3.9. *For $\alpha \geq \alpha_c$, $a_t = a \geq 1$ solution to $\nu_1^{\tilde{\mathcal{F}}}(a) = \alpha^{-1}$, γ_t such that $\|\mathbf{V}_{t+1}\|_{\text{op}} = 1$, with \mathbf{V}_{t+1} given by eq. (36), the state evolution has an unstable fixed point (\mathbf{M}, \mathbf{Q}) with*

$$\mathbf{M} = \mathbf{0}, \quad \mathbf{Q} \in \mathbb{S}_+^p \setminus \{\mathbf{0}\}, \tag{40}$$

correspondent to the eigenvalue $\lambda_b = a\gamma$.

The derivation of the Lemmas is outlined in Appendix C.

Conjecture 3.10. *In the high-dimensional limit $n, d \rightarrow \infty$, $n/d \rightarrow \alpha$, for $\alpha > \alpha_c$, the largest eigenvalue of $\underline{\mathbf{T}}$ converges to λ_s , defined in Lemma 3.8. In this regime, the symmetric spectral method, defined in (17), weakly recovers the signal. Moreover, the empirical spectral distribution of the pd eigenvalues of $\underline{\mathbf{T}}$ converges weakly almost surely to a density upper bounded by $\lambda_b < \lambda_s$ defined in Lemma 3.9.*

By construction, in multi-index models ($p > 1$), the tensor $\underline{\mathbf{T}}$, or equivalently its flattened matrix representation $\mathbf{flat}(\underline{\mathbf{T}})$, exhibits a highly structured form due to the presence of *repeated* entries from the measurement matrix \mathbf{X} . This intrinsic redundancy complicates its analysis using standard random matrix theory tools. Conjecture 3.10 based on results (3.8-3.9) and further supported by numerical simulations (see Fig. 2, 3), offers a novel framework for understanding the spectral properties of such matrices. Moreover, for any link function such that $\text{Cov}[\mathbf{z}|y]$ admits a common basis for all y , with real eigenvalues $\{\lambda_k(y) + 1\}_{k=1}^p$, the analysis of spectrum of $\mathbf{flat}(\underline{\mathbf{T}})$ can be

simplified following the arguments in Appendix D.2. Indeed, the symmetric spectral method reduces to the diagonalization of p matrices

$$\sum_{i \in \llbracket n \rrbracket} \frac{\lambda_k(y_i)}{\lambda_k(y_i) + 1} \mathbf{x}_i \mathbf{x}_i^T \in \mathbb{R}^{d \times d}, \quad k \in \llbracket p \rrbracket. \quad (41)$$

Their structure allows the use of the techniques in [Mondelli and Montanari \[2018\]](#), [Lu and Li \[2019\]](#) to analyze the spectrum, and could support the formalization of the results in [Conjecture 3.10](#) for this subset of problems.

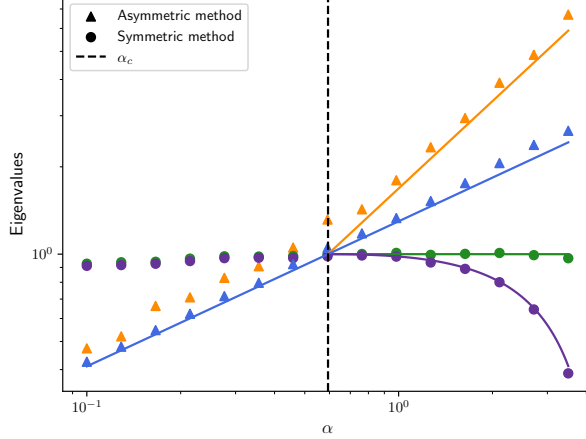


Figure 2: Largest eigenvalues (magnitude, if complex) of the tensors $\underline{\mathbf{L}}$ (triangles), $n = 5000$, and $\underline{\mathbf{T}}$ (circles), $d = 5000$, for the function $g(z_1, z_2) = z_1 z_2$, versus the sample complexity α . The orange and blue lines, respectively represent the values of the largest eigenvector α/α_c and the edge of the bulk $\sqrt{\alpha/\alpha_c}$ in [Conj. 3.5](#) for the asymmetric spectral method. The green and purple line correspond to the values of the largest eigenvalue λ_s and the edge of the bulk λ_b in [Conj. 3.10](#) for the symmetric spectral method.

3.3 Relation between the two spectral methods

As in the single-index setting, the tensors $\underline{\mathbf{L}}$ and $\underline{\mathbf{T}}$ are related by the following Proposition (proven in [App. F](#)).

Proposition 3.11.

1. Given an eigenpair $\gamma_{\underline{\mathbf{L}}} \geq 1, \Omega$ of $\underline{\mathbf{L}}$, and defining $\mathbf{W} := \mathbf{X}^T \underline{\mathbf{G}} \cdot \Omega$, then:

$$\underline{\mathbf{T}}_{\gamma_{\underline{\mathbf{L}}}} \cdot \mathbf{W} := \mathbf{X}^T \underline{\mathbf{G}} \cdot ((\underline{\mathbf{G}} + \gamma_{\underline{\mathbf{L}}} \mathbf{I})^{-1} \cdot (\mathbf{X} \mathbf{W})) = \mathbf{W}. \quad (42)$$

2. Given an eigenpair $\gamma_{\underline{\mathbf{T}}}, \mathbf{W}$ of $\underline{\mathbf{T}}$ and defining

$$\Omega := (\mathbf{I} + \underline{\mathbf{G}})^{-1} \cdot (\mathbf{X} \mathbf{W}), \quad (43)$$

then:

$$\underline{\mathbf{L}} \cdot \Omega = \gamma_{\underline{\mathbf{T}}} \Omega + (\gamma_{\underline{\mathbf{T}}} - 1) \underline{\mathbf{G}} \cdot \Omega. \quad (44)$$

Consequently, if there exists an eigenvector \mathbf{W} of $\underline{\mathbf{T}}$ with eigenvalue $\gamma_{\underline{\mathbf{T}}} = 1$, then Ω in [Eq. \(43\)](#) is an eigenvector of $\underline{\mathbf{L}}$ with eigenvalue $\gamma_{\underline{\mathbf{L}}} = \gamma_{\underline{\mathbf{T}}} = 1$.

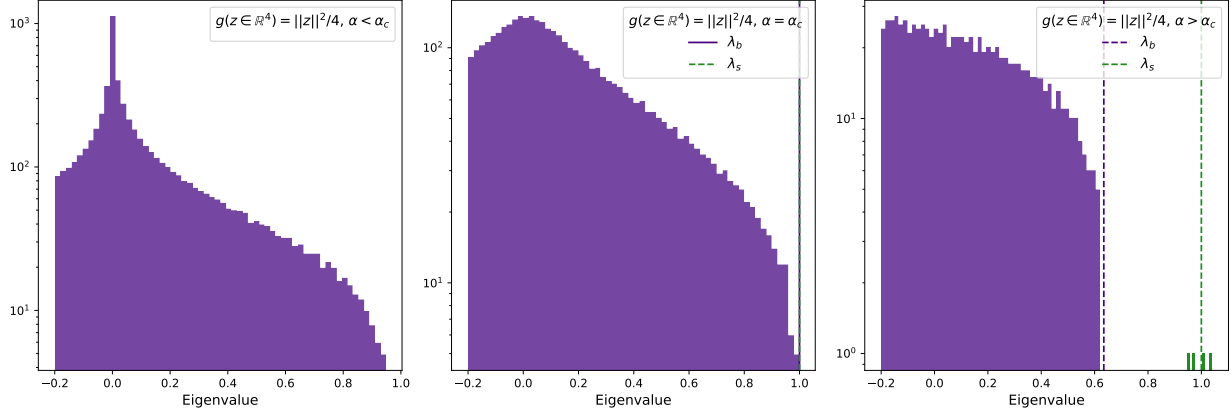


Figure 3: Distribution of the eigenvalues of $\underline{\mathbf{T}}$, $d = 10^4$, for the link function $g(\mathbf{z}) = p^{-1}\|\mathbf{z}\|^2$, $p = 4$. The critical threshold in $\alpha_c = 2$. The distribution is truncated on the left. **(Left)** $\alpha = 1 < \alpha_c$. **(Center)** $\alpha = \alpha_c$. **(Right)** $\alpha = 6 > \alpha_c$. As predicted by the state evolution framework, in this regime we observe four eigenvalues (highlighted in green) separated from the main bulk, centered around λ_s (green vertical line) obtained in Lemma 3.8. The vertical purple line correspond to the value λ_b provided in Lemma 3.9 as a bound for the bulk.

4 Examples

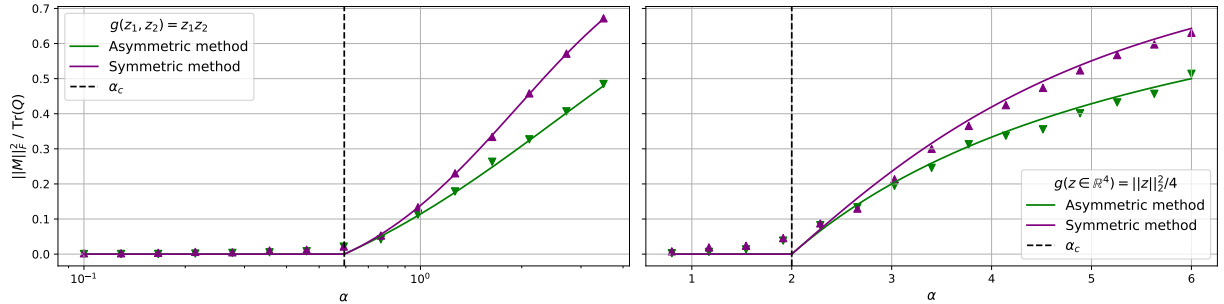


Figure 4: Overlap $\|\mathbf{M}\|_F^2 / \text{Tr}(\mathbf{Q})$ as a function of the sample complexity α . The dots represent numerical simulation results, computed for $n = 5000$ (for the asymmetric method) or $d = 5000$ (for the symmetric method) and averaging over 10 instances. **(Left)** Link function $g(z_1, z_2) = z_1 z_2$. Solid lines are obtained from state evolution predictions eq. (49,54). Dashed line at $\alpha_c \approx 0.59375$. **(Right)** Link function $g(\mathbf{z}) = p^{-1}\|\mathbf{z}\|^2$, $p = 4$. Solid lines are obtained from state evolution predictions eq. (47,54). Dashed line at $\alpha_c = 2$.

In this section we illustrate the framework introduced in Section 3 to predict the asymptotic performance of the spectral estimators (16,17) for specific examples of link functions, providing a comparison between our asymptotic analytical results and finite size numerical simulations for the overlap between the spectral estimators and the weights \mathbf{W}_* , defined as $m := \|\mathbf{M}\|_F / \sqrt{\text{Tr}(\mathbf{Q})}$, where \mathbf{M} and \mathbf{Q} are the overlap matrices defined in eq. (23) correspondent to the fixed points in Lemmas 3.3, 3.4, 3.8, 3.9. In Figure 4 we compare these theoretical predictions to numerical simulations at finite dimensions, respectively for the link functions $g(z_1, z_2) = z_1 z_2$ and $g(\mathbf{z}) = p^{-1}\|\mathbf{z}\|^2$. Additional numerical experiments are presented in Appendix D.

4.1 Asymmetric spectral method

We provide closed-form expressions for the overlap parameter $m := \|\mathbf{M}\|_{\mathbb{F}}/\sqrt{\text{Tr}(\mathbf{Q})}$ of the spectral estimator $\hat{\mathbf{W}}_{\underline{L}}$ (16), for a selection of examples of link functions. The details of the derivation are given in Appendix D.

- $g(z \in \mathbb{R})$ (single-index model):

$$\alpha_c = \left(\mathbb{E}_{y \sim Z} \left[(\text{Var}[z|y] - 1)^2 \right] \right)^{-1}, \quad (45)$$

$$m^2 = \left(\frac{\alpha - \alpha_c}{\alpha + \alpha_c^2 \mathbb{E}_{y \sim Z} \left[(\text{Var}[z|y] - 1)^3 \right]} \right)_+ \quad (46)$$

- $g(\mathbf{z}) = p^{-1} \|\mathbf{z}\|^2$:

$$\alpha_c = \frac{p}{2}, \quad m^2 = \left(\frac{(2\alpha - p)}{2(\alpha + 2)} \right)_+ \quad (47)$$

- $g(\mathbf{z}) = \text{sign}(z_1 z_2)$:

$$\alpha_c = \frac{\pi^2}{4}, \quad m^2 = \left(1 - \frac{\pi^2}{4\alpha} \right)_+ \quad (48)$$

- $g(\mathbf{z}) = \prod_{k=1}^p z_k$:

$$\alpha_c = \left(\mathbb{E}_{y \sim Z} [\lambda(y)^2] \right)^{-1}, \quad (49)$$

$$m^2 = \left(\frac{\alpha - \alpha_c}{\alpha + \alpha_c^2 \mathbb{E}_{y \sim Z} [\lambda(y)^3]} \right)_+, \quad (50)$$

where

$$\lambda(y) = \begin{cases} |y| \frac{K_1(|y|)}{K_0(|y|)} + y - 1, & p = 2 \\ \frac{2G_{0,p}^{p,0} \begin{pmatrix} y^2 2^{-p} \\ \mathbf{e}_p \end{pmatrix}}{G_{0,p}^{p,0} \begin{pmatrix} y^2 2^{-p} \\ \mathbf{0}_p \end{pmatrix}} - 1, & p \geq 3 \end{cases} \quad (51)$$

and the previous expression are written in terms of the modified Bessel function of the second kind and Meijer G-function, with the notations $\mathbf{0}_p \in \mathbb{R}^p = (0, \dots, 0)^T$ and $\mathbf{e}_p \in \mathbb{R}^p = (0, \dots, 0, 1)^T$.

- $g(z_1, z_2) = z_1 z_2^{-1}$: $\alpha_c = 1$, $m^2 = (1 - \alpha^{-1})_+$

4.2 Symmetric spectral method

We provide expressions for the overlap parameter $m := \|\mathbf{M}\|_{\mathbb{F}}/\sqrt{\text{Tr}(\mathbf{Q})}$ of the spectral estimator $\hat{\mathbf{W}}_{\underline{T}}$ (17), for a selection of examples of link functions. In all the following cases, the state evolution equations simplify, allowing to write the results as functionals of $\lambda : \mathbb{R} \rightarrow \mathbb{R}$, which is a specific to each problem:

- $g(z \in \mathbb{R})$ (single-index model): $\lambda(y) = \text{Var}[z|y] - 1$;
- $g(\mathbf{z}) = p^{-1} \|\mathbf{z}\|^2$: $\lambda(y) = y - 1$;

- $g(\mathbf{z}) = \text{sign}(z_1 z_2)$: $\lambda(y) = 2\pi^{-1}y$;
- $g(\mathbf{z}) = \prod_{k=1}^p z_k$: $\lambda(y)$ defined in eq. (51).

For all these example, the value α_c can be found in Section 4.1. For $\alpha > \alpha_c$, consider a and γ solutions of

$$\mathbb{E}_{y \sim \mathbf{Z}} \left[\frac{\lambda(y)^2}{a(1 + \lambda(y)) - \lambda(y)} \right] = \frac{1}{\alpha} \quad (52)$$

$$\gamma = 1 + \alpha \mathbb{E}_{y \sim \mathbf{Z}} \left[\frac{\lambda(y)}{a(1 + \lambda(y)) - \lambda(y)} \right]. \quad (53)$$

Then, for any α , the overlap $m := \|\mathbf{M}\|_{\text{F}} / \sqrt{\text{Tr}(\mathbf{Q})}$ is given by

$$m^2 = \left(\frac{1 - \alpha \mathbb{E}_{y \sim \mathbf{Z}} [\lambda^2(y) (a(1 + \lambda(y)) - \lambda(y))^{-2}]}{1 + \alpha \mathbb{E}_{y \sim \mathbf{Z}} [\lambda^3(y) (a(1 + \lambda(y)) - \lambda(y))^{-2}]} \right)_+, \quad (54)$$

which is strictly positive $\forall \alpha > \alpha_c$. Additional details on the derivation of this result can be found in Appendix E.

5 Conclusion and Perspectives

In this work, we tackled weak recovery in high-dimensional multi-index models via spectral methods, deriving two estimators inspired by a linearization of AMP. We showed they achieve the optimal reconstruction threshold, closing a key gap in prior approaches that required additional side information. Our analysis establishes that above the critical sample complexity, the leading eigenvectors of the proposed spectral operators align with the ground-truth subspace, echoing the BBP transition in random matrix theory.

This work advances our understanding of weak subspace recovery in multi-index models and provides a principled framework for designing optimal spectral estimators. It bridges ideas from random matrix theory, approximate message passing, and neural feature learning.

Several directions remain open. A random matrix theory analysis of our spectral analysis — which requires a challenging control of the spectral norms — could be used to prove the two conjectures. Extending our AMP linearization to higher-order schemes, such as the Kikuchi hierarchy, may unlock insights into harder generative exponent problems, including the notorious sparse parity function. We hope this work sparks further research at the intersection of spectral methods and high-dimensional inference.

Acknowledgements

The authors would like to thank Antoine Maillard, Benjamin Aubin and Lenka Zdeborova for early discussions on this problems in Santa Barbara. This research was supported in part by grant NSF PHY-2309135 to the Kavli Institute for Theoretical Physics (KITP), by the Swiss National Science Foundation under grant SNSF OperaGOST (grant number 200390) and by the French government, managed by the National Research Agency (ANR), under the France 2030 program with the reference "ANR-23-IACL-0008" and the Choose France - CNRS AI Rising Talents program.

References

Emmanuel Abbe, Enric Boix Adsera, and Theodor Misiakiewicz. The merged-staircase property: a necessary and nearly sufficient condition for sgd learning of sparse functions on two-layer neural networks. In *Conference on Learning Theory*, pages 4782–4887. PMLR, 2022.

Emmanuel Abbe, Enric Boix Adsera, and Theodor Misiakiewicz. Sgd learning on neural networks: leap complexity and saddle-to-saddle dynamics. In *The Thirty Sixth Annual Conference on Learning Theory*, pages 2552–2623. PMLR, 2023.

Luca Arnaboldi, Ludovic Stephan, Florent Krzakala, and Bruno Loureiro. From high-dimensional & mean-field dynamics to dimensionless odes: A unifying approach to sgd in two-layers networks. In *The Thirty Sixth Annual Conference on Learning Theory*, pages 1199–1227. PMLR, 2023.

Luca Arnaboldi, Yatin Dandi, Florent Krzakala, Bruno Loureiro, Luca Pesce, and Ludovic Stephan. Online learning and information exponents: On the importance of batch size, and time/complexity tradeoffs. *arXiv preprint arXiv:2406.02157*, 2024a.

Luca Arnaboldi, Yatin Dandi, Florent Krzakala, Luca Pesce, and Ludovic Stephan. Repetita iuvant: Data repetition allows sgd to learn high-dimensional multi-index functions. *arXiv preprint arXiv:2405.15459*, 2024b.

Luca Arnaboldi, Florent Krzakala, Bruno Loureiro, and Ludovic Stephan. Escaping mediocrity: how two-layer networks learn hard generalized linear models with sgd, 2024c.

Gerard Ben Arous, Reza Gheissari, and Aukosh Jagannath. Online stochastic gradient descent on non-convex losses from high-dimensional inference. *Journal of Machine Learning Research*, 22(106):1–51, 2021.

Benjamin Aubin, Antoine Maillard, Florent Krzakala, Nicolas Macris, Lenka Zdeborová, et al. The committee machine: Computational to statistical gaps in learning a two-layers neural network. *Advances in Neural Information Processing Systems*, 31, 2018.

Benjamin Aubin, Bruno Loureiro, Antoine Maillard, Florent Krzakala, and Lenka Zdeborová. The spiked matrix model with generative priors. *Advances in Neural Information Processing Systems*, 32, 2019.

Dmitry Babichev and Francis Bach. Slice inverse regression with score functions. *Electronic Journal of Statistics*, 12(1):1507 – 1543, 2018. doi: 10.1214/18-EJS1428. URL <https://doi.org/10.1214/18-EJS1428>.

Jinho Baik, Gérard Ben Arous, and Sandrine Péché. Phase transition of the largest eigenvalue for nonnull complex sample covariance matrices. 2005.

Jean Barbier, Florent Krzakala, Nicolas Macris, Léo Miolane, and Lenka Zdeborová. Optimal errors and phase transitions in high-dimensional generalized linear models. *Proceedings of the National Academy of Sciences*, 116(12):5451–5460, 2019. doi: 10.1073/pnas.1802705116. URL <https://www.pnas.org/doi/abs/10.1073/pnas.1802705116>.

Mohsen Bayati and Andrea Montanari. The dynamics of message passing on dense graphs, with applications to compressed sensing. *IEEE Transactions on Information Theory*, 57(2):764–785, 2011. doi: 10.1109/TIT.2010.2094817.

Raphaël Berthier, Andrea Montanari, and Kangjie Zhou. Learning time-scales in two-layers neural networks. *Foundations of Computational Mathematics*, pages 1–84, 2024.

Alberto Bietti, Joan Bruna, and Loucas Pillaud-Vivien. On learning gaussian multi-index models with gradient flow, 2023. URL <https://arxiv.org/abs/2310.19793>.

Michael Celentano, Andrea Montanari, and Yuchen Wu. The estimation error of general first order methods. In *Conference on Learning Theory*, pages 1078–1141. PMLR, 2020.

Elizabeth Collins-Woodfin, Courtney Paquette, Elliot Paquette, and Inbar Seroussi. Hitting the high-dimensional notes: An ode for sgd learning dynamics on glms and multi-index models. *Information and Inference: A Journal of the IMA*, 13(4):iaae028, 2024.

Alex Damian, Loucas Pillaud-Vivien, Jason D. Lee, and Joan Bruna. Computational-statistical gaps in gaussian single-index models, 2024. URL <https://arxiv.org/abs/2403.05529>.

Alexandru Damian, Jason Lee, and Mahdi Soltanolkotabi. Neural networks can learn representations with gradient descent. In *Conference on Learning Theory*, pages 5413–5452. PMLR, 2022.

Yatin Dandi, Florent Krzakala, Bruno Loureiro, Luca Pesce, and Ludovic Stephan. How two-layer neural networks learn, one (giant) step at a time. *Journal of Machine Learning Research*, 25(349):1–65, 2024a.

Yatin Dandi, Emanuele Troiani, Luca Arnaboldi, Luca Pesce, Lenka Zdeborová, and Florent Krzakala. The benefits of reusing batches for gradient descent in two-layer networks: Breaking the curse of information and leap exponents. *arXiv preprint arXiv:2402.03220*, 2024b.

David L Donoho, Arian Maleki, and Andrea Montanari. Message-passing algorithms for compressed sensing. *Proceedings of the National Academy of Sciences*, 106(45):18914–18919, 2009.

Alyson K Fletcher and Sundeep Rangan. Iterative reconstruction of rank-one matrices in noise. *Information and Inference: A Journal of the IMA*, 7(3):531–562, 2018.

Jerome H Friedman and Werner Stuetzle. Projection pursuit regression. *Journal of the American statistical Association*, 76(376):817–823, 1981.

Alice Guionnet, Justin Ko, Florent Krzakala, Pierre Mergny, and Lenka Zdeborová. Spectral phase transitions in non-linear wigner spiked models. *arXiv preprint arXiv:2310.14055*, 2023.

Jun-Ting Hsieh, Pravesh K Kothari, and Sidhanth Mohanty. A simple and sharper proof of the hypergraph moore bound. In *Proceedings of the 2023 Annual ACM-SIAM Symposium on Discrete Algorithms (SODA)*, pages 2324–2344. SIAM, 2023.

Adel Javanmard and Andrea Montanari. State evolution for general approximate message passing algorithms, with applications to spatial coupling. *Information and Inference: A Journal of the IMA*, 2(2):115–144, 2013.

Florent Krzakala, Cristopher Moore, Elchanan Mossel, Joe Neeman, Allan Sly, Lenka Zdeborová, and Pan Zhang. Spectral redemption in clustering sparse networks. *Proceedings of the National Academy of Sciences*, 110(52):20935–20940, 2013.

Jason D Lee, Kazusato Oko, Taiji Suzuki, and Denny Wu. Neural network learns low-dimensional polynomials with sgd near the information-theoretic limit. *arXiv preprint arXiv:2406.01581*, 2024.

Thibault Lesieur, Florent Krzakala, and Lenka Zdeborová. Constrained low-rank matrix estimation: Phase transitions, approximate message passing and applications. *Journal of Statistical Mechanics: Theory and Experiment*, 2017(7):073403, 2017.

Yue M Lu and Gen Li. Phase transitions of spectral initialization for high-dimensional non-convex estimation. *Information and Inference: A Journal of the IMA*, 9(3):507–541, 11 2019. ISSN 2049-8772. doi: 10.1093/imaiai/iaz020. URL <https://doi.org/10.1093/imaiai/iaz020>.

Wangyu Luo, Wael Alghamdi, and Yue M. Lu. Optimal spectral initialization for signal recovery with applications to phase retrieval. *IEEE Transactions on Signal Processing*, 67(9):2347–2356, 2019. doi: 10.1109/TSP.2019.2904918.

Antoine Maillard, Florent Krzakala, Yue M. Lu, and Lenka Zdeborova. Construction of optimal spectral methods in phase retrieval. In Joan Bruna, Jan Hesthaven, and Lenka Zdeborova, editors, *Proceedings of the 2nd Mathematical and Scientific Machine Learning Conference*, volume 145 of *Proceedings of Machine Learning Research*, pages 693–720. PMLR, 16–19 Aug 2022. URL <https://proceedings.mlr.press/v145/maillard22a.html>.

Marco Mondelli and Andrea Montanari. Fundamental limits of weak recovery with applications to phase retrieval. In Sébastien Bubeck, Vianney Perchet, and Philippe Rigollet, editors, *Proceedings of the 31st Conference On Learning Theory*, volume 75 of *Proceedings of Machine Learning Research*, pages 1445–1450. PMLR, 06–09 Jul 2018. URL <https://proceedings.mlr.press/v75/mondelli18a.html>.

Marco Mondelli and Ramji Venkataramanan. Approximate message passing with spectral initialization for generalized linear models. In Arindam Banerjee and Kenji Fukumizu, editors, *Proceedings of The 24th International Conference on Artificial Intelligence and Statistics*, volume 130 of *Proceedings of Machine Learning Research*, pages 397–405. PMLR, 13–15 Apr 2021. URL <https://proceedings.mlr.press/v130/mondelli21a.html>.

Marco Mondelli, Christos Thrampoulidis, and Ramji Venkataramanan. Optimal combination of linear and spectral estimators for generalized linear models. *Foundations of Computational Mathematics*, 22(5):1513–1566, Oct 2022. ISSN 1615-3383. doi: 10.1007/s10208-021-09531-x. URL <https://doi.org/10.1007/s10208-021-09531-x>.

Andrea Montanari and Yuchen Wu. Statistically optimal firstorder algorithms: a proof via orthogonalization. *Information and Inference: A Journal of the IMA*, 13(4):iaae027, 2024.

Ali Reza Mousavi-Hosseini, Denny Wu, and Murat A. Erdogdu. Learning multi-index models with neural networks via mean-field langevin dynamics, 2024. URL <https://arxiv.org/abs/2408.07254>.

Aleksandr Pak, Justin Ko, and Florent Krzakala. Optimal algorithms for the inhomogeneous spiked wigner model. *Advances in Neural Information Processing Systems*, 36, 2024.

Amelia Perry, Alexander S Wein, Afonso S Bandeira, and Ankur Moitra. Optimality and sub-optimality of pca i: Spiked random matrix models. *The Annals of Statistics*, 46(5):2416–2451, 2018.

Sundeep Rangan. Generalized approximate message passing for estimation with random linear mixing. In *2011 IEEE International Symposium on Information Theory Proceedings*, pages 2168–2172. IEEE, 2011.

Sundeep Rangan, Philip Schniter, and Alyson K. Fletcher. Vector approximate message passing. In *2017 IEEE International Symposium on Information Theory (ISIT)*, page 1588–1592. IEEE Press, 2017. doi: 10.1109/ISIT.2017.8006797. URL <https://doi.org/10.1109/ISIT.2017.8006797>.

Alaa Saade, Florent Krzakala, and Lenka Zdeborová. Spectral density of the non-backtracking operator on random graphs. *Europhysics Letters*, 107(5):50005, 2014.

Philip Schniter, Sundeep Rangan, and Alyson K. Fletcher. Vector approximate message passing for the generalized linear model. In *2016 50th Asilomar Conference on Signals, Systems and Computers*, pages 1525–1529, 2016. doi: 10.1109/ACSSC.2016.7869633.

Berfin Simsek, Amire Bendjedou, and Daniel Hsu. Learning gaussian multi-index models with gradient flow: Time complexity and directional convergence. *arXiv preprint arXiv:2411.08798*, 2024.

Steven H Strogatz. Nonlinear dynamics and chaos: with applications to physics, biology, chemistry, and engineering (studies in nonlinearity). *Nonlinear Dynamics and Chaos: With Applications to Physics, Biology, Chemistry, and Engineering (Studies in Nonlinearity)*, 2001.

Emanuele Troiani, Yatin Dandi, Leonardo Defilippis, Lenka Zdeborová, Bruno Loureiro, and Florent Krzakala. Fundamental limits of weak learnability in high-dimensional multi-index models. *arXiv preprint arXiv:2405.15480*, 2024.

Rodrigo Veiga, Ludovic Stephan, Bruno Loureiro, Florent Krzakala, and Lenka Zdeborová. Phase diagram of stochastic gradient descent in high-dimensional two-layer neural networks. *Advances in Neural Information Processing Systems*, 35:23244–23255, 2022.

Ramji Venkataramanan, Kevin Kögler, and Marco Mondelli. Estimation in rotationally invariant generalized linear models via approximate message passing. In *International Conference on Machine Learning*, pages 22120–22144. PMLR, 2022.

Alexander S Wein, Ahmed El Alaoui, and Christopher Moore. The kikuchi hierarchy and tensor pca. In *2019 IEEE 60th Annual Symposium on Foundations of Computer Science (FOCS)*, pages 1446–1468. IEEE, 2019.

Ming Yuan. On the identifiability of additive index models. *Statistica Sinica*, pages 1901–1911, 2011.

Yihan Zhang, Hong Chang Ji, Ramji Venkataramanan, and Marco Mondelli. Spectral estimators for structured generalized linear models via approximate message passing (extended abstract). In Shipra Agrawal and Aaron Roth, editors, *Proceedings of Thirty Seventh Conference on Learning Theory*, volume 247 of *Proceedings of Machine Learning Research*, pages 5224–5230. PMLR, 30 Jun–03 Jul 2024. URL <https://proceedings.mlr.press/v247/zhang24c.html>.

A Generalized Approximate Message Passing algorithms

In this section we present a general version of the multi-dimensional Generalized Approximate Message Passing (GAMP) algorithm [Rangan \[2011\]](#), defined as the iterations

$$\boldsymbol{\Omega}^t = \mathbf{X} \mathbf{f}_{in}^t(\mathbf{B}^t) - \mathbf{g}_{out}^{t-1}(\boldsymbol{\Omega}^{t-1}, \mathbf{y}) \mathbf{V}_t^T, \quad (55)$$

$$\mathbf{B}^{t+1} = \mathbf{X}^T \mathbf{g}_{out}^t(\boldsymbol{\Omega}^t, \mathbf{y}) - \mathbf{f}_{in}^t(\mathbf{B}^t) \mathbf{A}_t^T \quad (56)$$

and $\hat{\mathbf{W}}^{t+1} = \mathbf{f}_{in}^{t+1}(\mathbf{B}^{t+1})$. The *denoiser* functions $\mathbf{f}_{in}^t : \mathbb{R}^p \rightarrow \mathbb{R}^p$ and $\mathbf{g}_{out}^t : \mathbb{R}^p \times \mathbb{R} \rightarrow \mathbb{R}^p$ are vector-valued mappings acting row-wise respectively on $\mathbf{b}_j \in \mathbb{R}^p = \mathbf{B}_j$ and $\boldsymbol{\omega}_i \in \mathbb{R}^p = \boldsymbol{\Omega}_i$ and the *Onsager terms* are given by

$$\mathbf{A}_t = \frac{1}{d} \sum_{i=1}^n \nabla_{\boldsymbol{\omega}_i} \mathbf{g}_{out}^t(\boldsymbol{\omega}_i, y_i), \quad \mathbf{V}_t = \frac{1}{d} \sum_{j=1}^d \nabla_{\mathbf{b}_j} \mathbf{f}_{in}^t(\mathbf{b}_j). \quad (57)$$

Therefore, the algorithm is uniquely determined by the choice of denoisers. For instance, the optimal GAMP for Gaussian multi-index models, derived in [Aubin et al. \[2018\]](#), is given by

$$\mathbf{g}_{out}^t(\boldsymbol{\omega}, y) = \mathbf{V}_t^{-1} \mathbb{E}_{\mathbf{z} \sim \mathbf{N}(\boldsymbol{\omega}, \mathbf{V}_t)}[(\mathbf{z} - \boldsymbol{\omega}) \mathbf{P}(y|\mathbf{z})], \quad \mathbf{f}_{in}^t(\mathbf{b}) = \left(\mathbf{I}_p - \frac{1}{d} \sum_{i=1}^n \nabla_{\boldsymbol{\omega}_i} \mathbf{g}_{out}^t(\boldsymbol{\omega}_i, y_i) \right)^{-1} \mathbf{b}, \quad (58)$$

A.1 Linear GAMP

In this manuscript we focus on a special type of GAMP algorithms that have linear denoiser functions

$$\mathbf{g}_{out}^t(\boldsymbol{\omega}, y) = \mathbf{G}^t(y) \boldsymbol{\omega}, \quad \mathbf{f}_{in}^t(\mathbf{b}) = \mathbf{V}^t \mathbf{b}, \quad (59)$$

namely

$$\boldsymbol{\Omega}^t = \mathbf{X} \hat{\mathbf{W}}^t - \underline{\mathbf{G}}^{t-1} \cdot \boldsymbol{\Omega}^{t-1} \mathbf{V}_t^T, \quad (60)$$

$$\hat{\mathbf{W}}^{t+1} = \left(\mathbf{X}^T \underline{\mathbf{G}} \cdot \boldsymbol{\Omega}^t - \hat{\mathbf{W}}^t \mathbf{A}_t^T \right) \mathbf{V}_{t+1}^T, \quad (61)$$

where $G_{ikjh} = \delta_{ij}[\mathbf{G}(y_i)]_{kh}$ and

$$\mathbf{A} = d^{-1} \sum_{i \in \llbracket n \rrbracket} \mathbf{G}(y_i) \xrightarrow{n, d \rightarrow \infty} \alpha \mathbb{E}_{\mathbf{y} \sim \mathbf{Z}}[\mathbf{G}(\mathbf{y})]. \quad (62)$$

A particular example of Linear GAMP is the one obtained linearizing the denoiser functions (58) around the uninformed fixed point of the algorithm $\mathbf{b} = 0$, $\boldsymbol{\omega} = \mathbf{0}$ and $\mathbf{V} = \mathbf{I}$. We obtain a Linear GAMP with

$$\mathbf{G}(y) = \text{Cov}[\mathbf{z}|y] - \mathbf{I}, \quad \mathbf{V} = \mathbf{I} \quad (63)$$

and

$$\mathbf{A} = \alpha \mathbb{E}_{\mathbf{y} \sim \mathbf{Z}}[\mathbf{G}(\mathbf{y})] = \alpha \mathbb{E}_{\mathbf{y} \sim \mathbf{Z}} \mathbb{E}[\mathbf{z} \mathbf{z}^T | \mathbf{y}] - \alpha \mathbf{I} = \alpha \mathbb{E}_{\mathbf{z} \sim \mathbf{N}(\mathbf{0}, \mathbf{I})}[\mathbf{z} \mathbf{z}^T] - \alpha \mathbf{I} = \mathbf{0}. \quad (64)$$

A.2 State Evolution of Linear GAMP

One of the main advantages provided by the Approximate Message Passing algorithm is the possibility to track the value of low-dimensional functions of the iterates at all finite times, in the high-dimensional limit, through a set of iterative equations denoted as *state evolution* [Javanmard and Montanari \[2013\]](#). In particular, we are interested to the following overlap matrices

$$\mathbf{M}^t := \frac{1}{d} \left(\hat{\mathbf{W}}^t \right)^T \mathbf{W}_*, \quad \mathbf{Q}^t := \frac{1}{d} \left(\hat{\mathbf{W}}^t \right)^T \hat{\mathbf{W}}^t, \quad (65)$$

that characterize respectively the alignment between $\hat{\mathbf{W}}^t$ and the weights \mathbf{W}_* and the norm of $\hat{\mathbf{W}}^t$. In this appendix we present the state evolution equations for the GAMP algorithm (60, 61) with linear denoiser functions, while we refer to [Aubin et al. \[2018\]](#) for a complete derivation in more general settings:

$$\mathbf{M}^{t+1} = \mathbf{V}_t \hat{\mathbf{M}}^t, \quad \mathbf{Q}^{t+1} = \mathbf{V}_t \left(\hat{\mathbf{M}}^t (\hat{\mathbf{M}}^t)^T + \hat{\mathbf{Q}}^t \right) \mathbf{V}_t^T, \quad (66)$$

with the auxiliary matrices given by

$$\hat{\mathbf{M}}^t = \alpha \mathbb{E}_{y \sim \mathbf{Z}} [\mathbf{G}(y) \mathbf{M}^t (\text{Cov}[\mathbf{z}|y] - \mathbf{I})], \quad (67)$$

$$\hat{\mathbf{Q}}^t = \alpha \left(\mathbb{E}_{y \sim \mathbf{Z}} [\mathbf{G}(y) \mathbf{M}^t (\text{Cov}[\mathbf{z}|y] - \mathbf{I}) \mathbf{M}^T \mathbf{G}(y)^T] + \mathbb{E}_{y \sim \mathbf{Z}} [\mathbf{G}(y) \mathbf{Q}^t \mathbf{G}(y)^T] \right). \quad (68)$$

B Derivation of the main results - Asymmetric spectral method

Consider the following generalized power iteration algorithm

$$\boldsymbol{\Omega}^t = \gamma^{-1} \underline{\mathbf{L}} \cdot \boldsymbol{\Omega}^{t-1}, \quad (69)$$

$$\hat{\mathbf{W}}^{t+1} = \gamma^{-1} \mathbf{X}^T \underline{\mathbf{G}} \cdot \boldsymbol{\Omega}^t, \quad (70)$$

with $\underline{\mathbf{G}}$ defined in eq. (14). Given the principal eigenpair $\gamma_1, \boldsymbol{\Omega}_1$ of $\underline{\mathbf{L}}$, the spectral estimator defined in Definition 16 is a fixed point of this algorithm for $\gamma = \gamma_1$ and $\boldsymbol{\Omega} \propto \boldsymbol{\Omega}_1 \frac{\gamma_1 \sqrt{d}}{\|\mathbf{X}^T \underline{\mathbf{G}} \cdot \boldsymbol{\Omega}_1\|}$. Interestingly, the above algorithm is a linear GAMP, with denoiser functions $\mathbf{g}_{\text{out}}^t(\boldsymbol{\omega}, y) = (\text{Cov}[\mathbf{z}|y] - \mathbf{I})\boldsymbol{\omega}$ and $\mathbf{f}_{\text{in}}^t(\mathbf{b}) = \gamma^{-1} \mathbf{b}$, $\forall t$, and Onsager terms

$$\mathbf{A}_t \xrightarrow{n \rightarrow \infty} \alpha \mathbb{E}_{y \sim \mathbf{Z}} \mathbb{E}[\mathbf{z} \mathbf{z}^T | y] - \alpha \mathbf{I} = \mathbf{0}, \quad (71)$$

as already shown in (64), and $\mathbf{V}_t = \gamma^{-1} \mathbf{I}$. In fact, we can rewrite the generalized power iteration algorithm as

$$\boldsymbol{\Omega}^t = \gamma^{-1} (\mathbf{X} \mathbf{X}^T - \mathbf{I}_n) \underline{\mathbf{G}} \cdot \boldsymbol{\Omega}^{t-1} = \mathbf{X} (\gamma^{-1} \mathbf{B}^t) - \gamma^{-1} \underline{\mathbf{G}} \cdot \boldsymbol{\Omega}^{t-1}, \quad (72)$$

$$\mathbf{B}^{t+1} = \mathbf{X}^T \underline{\mathbf{G}} \cdot \boldsymbol{\Omega}^t, \quad (73)$$

$$\hat{\mathbf{W}}^{t+1} = \gamma^{-1} \mathbf{B}^{t+1}. \quad (74)$$

This algorithm does not offer any particular advantage for the practical computation of the spectral estimator compared to other algorithms for estimating the principal eigenvector. However, as an Approximate Message Passing algorithm, it enables to track low-dimensional functions of the iterate $\hat{\mathbf{W}}^t$ via the associated state evolution. Specifically, we will analyze the weak recovery properties of the spectral method by studying the convergence of the state evolution equations

$$\mathbf{M}^{t+1} = \frac{\alpha}{\gamma} \mathcal{F}(\mathbf{M}^t) \quad (75)$$

$$\mathbf{Q}^{t+1} = \mathbf{M}^t (\mathbf{M}^t)^T + \frac{\alpha}{\gamma^2} (\mathcal{G}(\mathbf{M}^t) + \mathcal{F}(\mathbf{Q}^t)) \quad (76)$$

where

$$\mathcal{F}(\mathbf{M}) := \mathbb{E}_y[(\text{Cov}[\mathbf{z}|y] - \mathbf{I})\mathbf{M}(\text{Cov}[\mathbf{z}|y] - \mathbf{I})], \quad (77)$$

$$\mathcal{G}(\mathbf{M}) := \mathbb{E}_y[(\text{Cov}[\mathbf{z}|y] - \mathbf{I})\mathbf{M}(\text{Cov}[\mathbf{z}|y] - \mathbf{I})\mathbf{M}^T(\text{Cov}[\mathbf{z}|y] - \mathbf{I})]. \quad (78)$$

The linear operator $\mathcal{F} : \mathbb{R}^{p \times p} \rightarrow \mathbb{R}^{p \times p}$ is symmetric, therefore it admits p^2 eigenpairs $(\nu_k \in \mathbb{R}, \mathbf{M}_k)_{k \in [p^2]}$ such that $\mathcal{F}(\mathbf{M}_k) = \nu_k \mathbf{M}_k$ and the (matrix) eigenvectors are an orthonormal basis of $\mathbb{R}^{p \times p}$. In particular, Lemma 2.2 implies that $\nu_1 := \max_k \nu_k > 0$ and $\mathbf{M}_1 \in \mathbb{S}_+^p$. This eigenvalue corresponds to the inverse of the critical sample complexity α_c , defined in 2.2. We can distinguish between two kind of fixed points:

1. **Informed fixed points.** For $\gamma = \alpha \nu_k$ ($\nu_k \neq 0$), $\mathbf{M} \propto \mathbf{M}_k$, is a non-zero fixed point for eq. (75). In particular, we are interested to the fixed point correspondent to the largest γ , *i.e.* $\mathbf{M} \propto \mathbf{M}_1$. For $\alpha > \alpha_c$ and $\gamma = \alpha/\alpha_c > 1$, the largest eigenvalue of $\alpha \mathcal{F}(\cdot)$ is equal to one and any $\mathbf{M} \propto \mathbf{M}_1$ is a stable fixed point. Moreover, eq. (76) at convergence:

$$\mathbf{Q} = \mathbf{M}^2 + \frac{\alpha_c^2}{\alpha} (m^2 \mathcal{G}(\mathbf{M}) + \mathcal{F}(\mathbf{Q})) \implies \quad (79)$$

$$\text{Tr}(\mathbf{Q}) = \|\mathbf{M}\|_{\text{F}}^2 \left(1 + \frac{\alpha_c^2}{\alpha} \underbrace{\text{Tr} \left(\mathcal{G} \left(\frac{\mathbf{M}}{\|\mathbf{M}\|_{\text{F}}} \right) \right)}_{\geq 0} \right) + \frac{\alpha_c^2}{\alpha} \underbrace{\text{Tr}(\mathcal{F}(\mathbf{Q}))}_{\leq \nu_1 \text{Tr}(\mathbf{Q})} \implies \quad (80)$$

$$\|\mathbf{M}\|_{\text{F}}^2 \geq \left(1 - \frac{\alpha_c}{\alpha} \right) \text{Tr}(\mathbf{Q}) \left(1 + \frac{\alpha_c^2}{\alpha} \text{Tr} \left(\mathcal{G} \left(\frac{\mathbf{M}}{\|\mathbf{M}\|_{\text{F}}} \right) \right) \right)^{-1} > 0, \quad (81)$$

where in eq. (80) we used

$$\text{Tr} \mathcal{F} \left(\mathbf{Q} = \sum_{k \in [p^2]} c_k \mathbf{M}_k \right) = \text{Tr} \sum_{k \in [p^2]} c_k \nu_k \mathbf{M}_k \leq \nu_1 \text{Tr} \mathbf{Q}. \quad (82)$$

Therefore, the correspondent estimator weakly recovers \mathbf{W}_* .

2. **Uninformed fixed point.** Initializing GAMP in a subspace orthogonal to the signal, *i.e.* $\mathbf{M}^0 = \mathbf{0}$,

$$\mathbf{Q} = \gamma^{-2} \alpha \mathcal{F}(\mathbf{Q}), \quad (83)$$

therefore, for $\gamma = \sqrt{\alpha \nu_1}$, $\mathbf{M} = \mathbf{0}$, $\mathbf{Q} = \mathbf{M}_1 \in \mathbb{S}_+^p \setminus \{\mathbf{0}\}$ is a fixed point of the state evolution. Note that, since the largest eigenvalue of $\alpha \mathcal{F}(\cdot)$ is larger than one, such fixed point is unstable. Since the proposed GAMP is equivalent to a generalized power iteration algorithm, normalized by the constant $\gamma \in \mathbb{R}$, it converges only if γ corresponds to the absolute value of the eigenvalue with largest magnitude in the subspace of initialization.

C Derivation of the main results - Symmetric spectral method

Similarly to what we have done in the previous section, we introduce a GAMP algorithm that will serve as a framework to study the properties of the spectral estimator defined in (17).

Definition C.1. Consider the Generalized Approximate Message Passing algorithm defined by the denoiser functions

$$\mathbf{g}_\text{out}^t(\mathbf{y}, \boldsymbol{\omega}) = \mathcal{T}(y) \mathbf{V}_t^T (a_t \mathbf{I} - \mathbf{V}_t \mathcal{T}(y) \mathbf{V}_t^T)^{-1} \boldsymbol{\omega}, \quad \mathbf{f}_{in}^t(\mathbf{b}) = (\gamma_t \mathbf{V}_t^T - \mathbf{A}_t)^{-1} \mathbf{b}, \quad (84)$$

where $\mathcal{T}(y)$ is the preprocessing function defined in (33) and a_t, γ_t parameters to be fixed.

Dropping the time index for the fixed-point variables and parameters, and defining $\underline{\mathbf{T}}_{\mathbf{V}}$ as

$$\underline{\mathbf{T}}_{\mathbf{V}} \cdot \boldsymbol{\Omega} = \mathbf{V} \underline{\mathbf{T}} \cdot \boldsymbol{\Omega}, \quad (85)$$

the fixed points satisfy

$$\boldsymbol{\Omega} = \mathbf{X} \hat{\mathbf{W}} - \underline{\mathbf{T}}_{\mathbf{V}} \cdot \boldsymbol{\Omega} \implies \boldsymbol{\Omega} = (\underline{\mathbf{I}} + \underline{\mathbf{T}}_{\mathbf{V}})^{-1} \cdot (\mathbf{X} \hat{\mathbf{W}}), \quad (86)$$

$$\hat{\mathbf{W}}(\gamma_t \mathbf{V} - \mathbf{A}^T) = \mathbf{X} \mathbf{X}^T \underline{\mathbf{T}} \cdot \left((\underline{\mathbf{I}} + \underline{\mathbf{T}}_{\mathbf{V}})^{-1} \cdot (\mathbf{X} \hat{\mathbf{W}}) \right) - \hat{\mathbf{W}} \mathbf{A}^T \implies a \gamma_t \hat{\mathbf{W}} \mathbf{V} = \underline{\mathbf{T}} \cdot (\hat{\mathbf{W}} \mathbf{V}), \quad (87)$$

where we used

$$[\underline{\mathbf{T}} \cdot ((\underline{\mathbf{I}} + \underline{\mathbf{T}}_{\mathbf{V}})^{-1} \cdot \boldsymbol{\Omega})]_{i \cdot} = \mathcal{T}(y) \mathbf{V}^T (a \mathbf{I} - \mathbf{V} \mathcal{T}(y) \mathbf{V}^T)^{-1} [(\underline{\mathbf{I}} + \underline{\mathbf{T}}_{\mathbf{V}})^{-1} \boldsymbol{\Omega}]_{i \cdot} \quad (88)$$

$$= \mathcal{T}(y) \mathbf{V}^T (a \mathbf{I} - \mathbf{V} \mathcal{T}(y) \mathbf{V}^T)^{-1} (\mathbf{I} + \mathbf{V} \mathcal{T}(y) \mathbf{V}^T (a \mathbf{I} - \mathbf{V} \mathcal{T}(y) \mathbf{V}^T)^{-1})^{-1} \boldsymbol{\Omega}_{i \cdot} \quad (89)$$

$$= \mathcal{T}(y) \mathbf{V}^T (a \mathbf{I} - \mathbf{V} \mathcal{T}(y) \mathbf{V}^T + \mathbf{V} \mathcal{T}(y) \mathbf{V}^T)^{-1} \boldsymbol{\Omega}_{i \cdot} \quad (90)$$

$$= a^{-1} \mathcal{T}(y) \mathbf{V}^T \boldsymbol{\Omega}_{i \cdot} \quad (91)$$

Therefore, $\hat{\mathbf{W}} = \hat{\mathbf{W}} \underline{\mathbf{T}} \mathbf{V}^{-1}$ is a fixed point of the algorithm, for a_t and γ_t appropriately chosen, with eigenvalue given by $a_t \gamma_t$ at convergence.²

C.1 State Evolution

The state evolution equations of the overlap matrices are

$$\mathbf{M}^{t+1} = \alpha \mathcal{F}(\mathbf{M}^t; a_t, \mathbf{V}_t) \quad (92)$$

$$\mathbf{Q}^{t+1} = \mathbf{M}^t (\mathbf{M}^t)^T + \alpha (\mathcal{G}(\mathbf{M}^t; a_t, \mathbf{V}_t) + \tilde{\mathcal{F}}(\mathbf{Q}^t; a_t, \mathbf{V}_t)) \quad (93)$$

$$\mathbf{V}_{t+1} = (\gamma_t \mathbf{V}_t^T - \mathbf{A}_t)^{-1}, \quad (94)$$

$$\mathbf{A}_t = \alpha \mathbb{E}_{\mathbf{y} \sim \mathbf{Z}(\mathbf{y})} [\mathcal{T}(\mathbf{y}) \mathbf{V}_t^T (a_t - \mathbf{V}_t \mathcal{T}(\mathbf{y}) \mathbf{V}_t^T)^{-1}] \quad (95)$$

with

$$\mathcal{F}(\mathbf{M}; a, \mathbf{V}) := \mathbb{E}_{\mathbf{y} \sim \mathbf{Z}} [\mathbf{V} \mathcal{T}(\mathbf{y}) \mathbf{V}^T (a - \mathbf{V} \mathcal{T}(\mathbf{y}) \mathbf{V}^T)^{-1} \mathbf{M} (\text{Cov}[\mathbf{z}|\mathbf{y}] - \mathbf{I})], \quad (96)$$

$$\tilde{\mathcal{F}}(\mathbf{Q}; a, \mathbf{V}) := \mathbb{E}_{\mathbf{y} \sim \mathbf{Z}} [\mathbf{V} \mathcal{T}(\mathbf{y}) \mathbf{V}^T (a - \mathbf{V} \mathcal{T}(\mathbf{y}) \mathbf{V}^T)^{-1} \mathbf{Q} (a - \mathbf{V} \mathcal{T}(\mathbf{y}) \mathbf{V}^T)^{-1} \mathbf{V} \mathcal{T}(\mathbf{y}) \mathbf{V}^T] \quad (97)$$

²Note that the overlap matrices for this algorithm refer to $\hat{\mathbf{W}} \underline{\mathbf{T}} \mathbf{V}^{-1}$ and not directly to the spectral estimator itself. However, if $\|\mathbf{M}\|_{\text{F}} > 0$, the weak recovery condition is satisfied.

$$\mathcal{G}(\mathbf{M}; a, \mathbf{V}) := \mathbb{E}_{y \sim Z} [\mathbf{V} \mathcal{T}(y) \mathbf{V}^T (a - \mathbf{V} \mathcal{T}(y) \mathbf{V}^T)^{-1} \mathbf{M} (\text{Cov}[\mathbf{z}|y] - \mathbf{I}) \mathbf{M}^T (a - \mathbf{V} \mathcal{T}(y) \mathbf{V}^T)^{-1} \mathbf{V} \mathcal{T}(y) \mathbf{V}^T]. \quad (98)$$

Note that $\mathcal{F}(\cdot; a, \mathbf{V})$ is a symmetric linear operator on the space of $p \times p$ matrices, with respect to the inner product $\langle \mathbf{M}, \mathbf{M}' \rangle := \text{Tr}(\mathbf{M}^T \mathbf{M}')$:

$$\langle \mathcal{F}(\mathbf{M}; a, \mathbf{V}), \mathbf{M}' \rangle = \mathbb{E}_{y \sim Z} \text{Tr} [(\text{Cov}[\mathbf{z}|y] - \mathbf{I}) \mathbf{M}^T (a - \mathbf{V} \mathcal{T}(y) \mathbf{V}^T)^{-1} \mathbf{V} \mathcal{T}(y) \mathbf{V}^T \mathbf{M}'] \quad (99)$$

$$= \mathbb{E}_{y \sim Z} \text{Tr} [(a - \mathbf{V} \mathcal{T}(y) \mathbf{V}^T)^{-1} \mathbf{V} \mathcal{T}(y) \mathbf{V}^T \mathbf{M}' (\text{Cov}[\mathbf{z}|y] - \mathbf{I}) \mathbf{M}^T] \quad (100)$$

$$= \text{Tr} \mathbb{E}_{y \sim Z} [\mathbf{V} \mathcal{T}(y) \mathbf{V}^T (a - \mathbf{V} \mathcal{T}(y) \mathbf{V}^T)^{-1} \mathbf{M}' (\text{Cov}[\mathbf{z}|y] - \mathbf{I}) \mathbf{M}^T] \quad (101)$$

$$= \langle \mathcal{F}(\mathbf{M}'; a, \mathbf{V}), \mathbf{M} \rangle. \quad (102)$$

This implies that, for a, \mathbf{V} fixed, $\mathcal{F}(\cdot; a, \mathbf{V})$ has p^2 real eigenvalues $\{\nu_k(a, \mathbf{V})\}_{k \in \llbracket p^2 \rrbracket}$ and admits an orthonormal basis $\{\mathbf{M}_k(a, \mathbf{V})\}_{k \in \llbracket p^2 \rrbracket}$ of eigenvectors in $\mathbb{R}^{p \times p}$. Moreover, note that from the state evolution iterations, we can verify that $\mathbf{V}_t = \mathbf{V}_t^T \implies \mathbf{V}_{t+1} = \mathbf{V}_{t+1}^T$, therefore, we consider the matrix \mathbf{V}_t to be symmetric at all times. From the state evolution equations at convergence

$$\mathbf{V} = \sqrt{\gamma^{-1}} \left(\mathbf{I} + \alpha \mathbb{E}_{y \sim Z} [\mathbf{V} \mathcal{T}(y) \mathbf{V} (a - \mathbf{V} \mathcal{T}(y) \mathbf{V})^{-1}] \right)^{1/2} \implies \mathbf{V} \succ \mathbf{0}. \quad (103)$$

Furthermore, in order to bound the operator norm of \mathbf{V} , we choose γ_t such that $\|\mathbf{V}_{t+1}\|_{\text{op}} = 1$. We can distinguish the following cases:

- **Informed fixed points.** Choosing a_t such that

$$\max \left\{ \lim_{t \rightarrow \infty} \nu_k(a_t, \mathbf{V}_t) : k \in \llbracket p^2 \rrbracket \right\} = \alpha^{-1}, \quad (104)$$

then $\exists \mathbf{M} \neq \mathbf{0}$ stable fixed point of the state evolution, and, for $\alpha > \alpha_c$ ($a > 1$)

$$\text{Tr}(\mathbf{Q}) = \|\mathbf{M}\|_{\text{F}}^2 + \alpha \|\mathbf{M}\|_{\text{F}}^2 \text{Tr} \left(\mathcal{G} \left(\frac{\mathbf{M}}{\|\mathbf{M}\|_{\text{F}}}; a, \mathbf{V} \right) \right) + \alpha \text{Tr}(\tilde{\mathcal{F}}(\mathbf{Q}; a, \mathbf{V})) \implies \quad (105)$$

$$\|\mathbf{M}\|_{\text{F}} \geq \text{Tr}(\mathbf{Q}) - \alpha \text{Tr}(\tilde{\mathcal{F}}(\mathbf{Q}; a, \mathbf{V})) > 0, \quad (106)$$

where we used, introducing the auxiliary notation $\mathcal{L}(y, a, \mathbf{V}) = (\text{Cov}[\mathbf{z}|y](a \mathbf{V}^{-1} - \mathbf{V}) + \mathbf{V})^{-1}$

$$\begin{aligned} \text{Tr}(\tilde{\mathcal{F}}(\mathbf{Q}; a, \mathbf{V})) &= \mathbb{E}_{y \sim Z} \text{Tr} [\mathbf{V} \mathcal{T}(y) \mathbf{V} (a - \mathbf{V} \mathcal{T}(y) \mathbf{V})^{-1} \mathbf{Q} (a - \mathbf{V} \mathcal{T}(y) \mathbf{V})^{-1} \mathbf{V} \mathcal{T}(y) \mathbf{V}] \\ &= \mathbb{E}_y \text{Tr} [\mathbf{V} \mathcal{T}(y) \mathbf{V} (a - \mathbf{V} \mathcal{T}(y) \mathbf{V})^{-1} \mathbf{Q} \mathbf{V} (\text{Cov}[\mathbf{z}|y] - \mathbf{I}) \mathcal{L}(y, a, \mathbf{V})^T] \\ &\leq \mathbb{E}_y \text{Tr} [\mathbf{V} \mathcal{T}(y) \mathbf{V} (a - \mathbf{V} \mathcal{T}(y) \mathbf{V})^{-1} \mathbf{Q} \mathbf{V} (\text{Cov}[\mathbf{z}|y] - \mathbf{I})] \underbrace{\text{Tr} [\mathcal{L}(y, a, \mathbf{V})^T]}_{< \text{Tr}[\mathcal{L}(y, 1, \mathbf{V})^T] \leq 1} \\ &< \text{Tr} \mathbb{E}_y [\mathbf{V} \mathcal{T}(y) \mathbf{V} (a - \mathbf{V} \mathcal{T}(y) \mathbf{V})^{-1} \mathbf{Q} \mathbf{V} (\text{Cov}[\mathbf{z}|y] - \mathbf{I})] \\ &= \text{Tr}(\mathcal{F}(\mathbf{Q} \mathbf{V}; a, \mathbf{V})) \\ &\leq \alpha^{-1} \|\mathbf{V}^{1/2}\|_{\text{op}}^2 \text{Tr}(\mathbf{Q}) = \alpha^{-1} \text{Tr}(\mathbf{Q}),. \end{aligned}$$

together with $\text{Cov}[\mathbf{z}|y] \succ \mathbf{0}$ (a.s. over $y \sim Z$) and $\|\mathbf{V}\|_{\text{op}} = 1$.

- **Uninformed fixed points.** Initializing GAMP with $\mathbf{M}^0 = \mathbf{0}$, which is a fixed point of the state evolution,

$$\mathbf{Q} = \alpha \tilde{\mathcal{F}}(\mathbf{Q}; , \mathbf{V}),. \quad (107)$$

Similarly to $\mathcal{F}(\cdot; a, \mathbf{V})$, the symmetric operator $\tilde{\mathcal{F}}(\cdot; a, \mathbf{V})$ has p^2 real eigenvalues. Defining $\nu_1^{\tilde{\mathcal{F}}}(a)$ as its largest one, we notice that $\nu_1^{\tilde{\mathcal{F}}}(1) = \alpha_c^{-1}$ and $\nu_1^{\tilde{\mathcal{F}}}(a \rightarrow \infty) \rightarrow 0$. Therefore, for $\alpha > \alpha_c$, $\exists a > 1$ such that $\nu_1^{\tilde{\mathcal{F}}} = \alpha^{-1}$ and the state evolution has a fixed point $\mathbf{M} = \mathbf{0}$, $\mathbf{Q} \in \mathbb{S}_+^p \setminus \{\mathbf{0}\}$. Moreover, for such a , the largest eigenvalue of $\mathcal{F}(\cdot; a, \mathbf{V})$ is larger than α^{-1} , hence the uninformed fixed point is unstable for $\alpha > \alpha_c$. This can be shown repeating a similar argument as the one we have applied in eq. (106). Since the GAMP convergence equations correspond to a generalized power iteration of $\underline{\mathbf{T}}$, normalized by the eigenvalue $a\gamma$, the instability of the uninformed fixed point implies that it is associated to an eigenvector smaller than λ_s defined in Lemma 3.8.

D Details on examples - Asymmetric spectral method

D.1 Single-index models

The case of single-index models ($p = 1$) allows for significant simplifications, as

$$\mathcal{F}(M \in \mathbb{R}) = M \mathbb{E}_{y \sim \mathbf{z}} \left[(\text{Var}[z|y] - 1)^2 \right], \quad (108)$$

$$\mathcal{G}(M \in \mathbb{R}) = M^2 \mathbb{E}_{y \sim \mathbf{z}} \left[(\text{Var}[z|y] - 1)^3 \right]. \quad (109)$$

This leads to the well known expression for the critical weak recovery threshold [Barbier et al. \[2019\]](#), [Mondelli and Montanari \[2018\]](#), [Lu and Li \[2019\]](#), [Maillard et al. \[2022\]](#), [Damian et al. \[2024\]](#)

$$\alpha_c^{-1} = \mathbb{E}_{y \sim \mathbf{z}} \left[(\text{Var}[z|y] - 1)^2 \right], \quad (110)$$

and to the following result for the overlap parameter $m = M/\sqrt{Q}$

$$m^2 = \begin{cases} (\alpha - \alpha_c) \left(\alpha + \alpha_c^2 \mathbb{E}_{y \sim \mathbf{z}} \left[(\text{Var}[z|y] - 1)^3 \right] \right)^{-1}, & \alpha \geq \alpha_c \\ 0, & \alpha < \alpha_c \end{cases}. \quad (111)$$

D.2 $\text{Cov}[\mathbf{z}|y]$ jointly diagonalizable $\forall y$

In this section, we consider the ensemble of link functions g corresponding to a matrix $\text{Cov}[\mathbf{z}|y]$ that can be diagonalized with respect to the same basis of eigenvectors for all y : there exists an orthogonal matrix $\mathbf{U} \in \mathbb{R}^{p \times p} = (\mathbf{u}_1, \dots, \mathbf{u}_p)$ independent of y and real numbers $\lambda_k(y)$ such that

$$(\text{Cov}[\mathbf{z}|y] - \mathbf{I})\mathbf{u}_k = \lambda_k(y)\mathbf{u}_k, \quad k \in \llbracket p \rrbracket. \quad (112)$$

Consider a separate link function \bar{g} defined as $\bar{g}(\mathbf{Z}) := g(\mathbf{Uz})$, $\forall \mathbf{z} \in \mathbb{R}^p$. It is easy to show that g and \bar{g} share the same weak recovery properties, including the sample complexity threshold. Indeed, introducing temporarily the notations $\bar{Z}(y)$, $\bar{P}(y|\cdot)$, $\bar{\alpha}_c$, for the quantities related to \bar{g} , we have that

$$\bar{Z}(y) = (2\pi)^{-p/2} \int_{\mathbb{R}^p} e^{-1/2\mathbf{z}^T \mathbf{z}} \delta(y - g(\mathbf{Uz})) d\mathbf{z} \quad (113)$$

$$\stackrel{(\mathbf{z}' = \mathbf{Uz})}{=} (2\pi)^{-p/2} \int_{\mathbb{R}^p} e^{-1/2\mathbf{z}'^T \mathbf{U} \mathbf{U}^T \mathbf{z}'} \delta(y - g(\mathbf{Uz}')) d\mathbf{z}' = Z(y), \quad (114)$$

and similarly

$$\mathbb{E}_{\mathbf{z}}[\mathbf{z}\bar{P}(y|\mathbf{z})] = \mathbf{U}^T \mathbb{E}_{\mathbf{z}}[\mathbf{z}P(y|\mathbf{z})], \quad (115)$$

$$\mathbb{E}_{\mathbf{z}}[\mathbf{z}\mathbf{z}^T\bar{\mathbf{P}}(y|\mathbf{z})] = \mathbf{U}^T\mathbb{E}_{\mathbf{z}}[\mathbf{z}\mathbf{z}^T\mathbf{P}(y|\mathbf{z})]\mathbf{U} = \mathbf{U}^T\text{Cov}[\mathbf{z}|y]\mathbf{U} \quad (\text{diagonal}). \quad (116)$$

If $\mathbb{E}_{\mathbf{z}}[\mathbf{z}\mathbf{P}(y|\mathbf{z})] = \mathbf{0}$ almost surely for $y \sim Z$, the same applies to $\mathbb{E}_{\mathbf{z}}[\mathbf{z}\bar{\mathbf{P}}(y|\mathbf{z})]$, and both problems are non-trivial. In this case

$$\bar{\alpha}_c^{-1} = \max_{\|\mathbf{M}\|_F=1} \|\mathbb{E}_{y \sim \bar{Z}}[(\mathbb{E}_{\mathbf{z}}[\mathbf{z}\mathbf{z}^T\bar{\mathbf{P}}(y|\mathbf{z})] - \mathbf{I})\mathbf{M}(\mathbb{E}_{\mathbf{z}}[\mathbf{z}\mathbf{z}^T\bar{\mathbf{P}}(y|\mathbf{z})] - \mathbf{I})]\|_F \quad (117)$$

$$= \max_{\|\mathbf{M}\|_F=1} \|\mathbb{E}_{y \sim Z}[(\text{Cov}[\mathbf{z}|y] - \mathbf{I})\mathbf{U}\mathbf{M}\mathbf{U}^T(\text{Cov}[\mathbf{z}|y] - \mathbf{I})]\|_F \quad (118)$$

$$= \max_{\|\mathbf{M}'\|_F=1} \|\mathbb{E}_{y \sim Z}[(\text{Cov}[\mathbf{z}|y] - \mathbf{I})\mathbf{M}'(\text{Cov}[\mathbf{z}|y] - \mathbf{I})]\|_F = \alpha_c^{-1}. \quad (119)$$

Therefore, whenever we are in this setting, we can consider without loss of generality $(\text{Cov}[\mathbf{z}|y] - \mathbf{I}) = \text{diag}(\lambda_1(y), \dots, \lambda_p(y))$. The eigenpairs of the operator \mathcal{F} eq. (77) are given by

$$\nu_{(k,h)} = \mathbb{E}_y[\lambda_k(y)\lambda_h(y)], \quad \mathbf{M}_{(k,h)} \text{ with } [\mathbf{M}_{(k,h)}]_{\mu\nu} = \delta_{k\mu}\delta_{h\nu}, \quad \forall k, h \in \llbracket p \rrbracket, \quad (120)$$

with the critical sample complexity $\bar{\alpha}_c^{-1} = \nu_1 := \max_{k \in \llbracket p \rrbracket} \nu_{(k,k)}$ ³. If the maximum is achieved by more than one pair of indices, we expect that the matrix \mathbf{L} principal eigenvalue is degenerate, with degeneracy given by the cardinality of the set $\mathcal{I} = \{(k, h) \in \{1, \dots, p\}^2 \mid \nu_{(k,h)} = \alpha_c^{-1}\}$. Note that $\forall k, h, \nu_{(k,h)} = \nu_{(h,k)}$ and if $\nu_{(k,h)} = \max_{\mu \in \{k, h\}} \nu_{\mu\mu} \implies \nu_{(k,k)} = \nu_{(h,h)}$.⁴ The generic principal eigenvector of \mathcal{F} is given by $\mathbf{M} = \|\mathbf{M}\|_F \sum_{(k,h) \in \mathcal{I}} c_{(k,h)} \mathbf{M}_{(k,h)}$ with $\sum c_{(k,h)}^2 = 1$. We introduce the ansatz: \mathbf{Q} s.t. $\mathbf{Q}_{kk} \neq 0$ iff $(k, k) \in \mathcal{I}$; this implies $\text{Tr}(\mathcal{F}(\mathbf{Q})) = \sum_k \mathbb{E}[\lambda_k(y)^2]Q_{kk} = \alpha_c^{-1}\text{Tr}(\mathbf{Q})$. Eq. (80) becomes

$$\text{Tr}(\mathbf{Q}) = \|\mathbf{M}\|_F^2 \left(1 + \frac{\alpha_c^2}{\alpha} \sum_{(k,h) \in \mathcal{I}} c_{(k,h)}^2 \text{Tr}(\mathcal{G}(\mathbf{M}_{(k,h)})) \right) + \frac{\alpha_c^2}{\alpha} \text{Tr}(\mathcal{F}(\mathbf{Q})) \implies \quad (121)$$

$$\text{Tr}(\mathbf{Q}) = \|\mathbf{M}\|_F^2 \left(1 + \frac{\alpha_c^2}{\alpha} \sum_{(k,h) \in \mathcal{I}} c_{(k,h)}^2 \mathbb{E}_y[\lambda_k(y)^2 \lambda_h(y)] \right) + \frac{\alpha_c}{\alpha} \text{Tr}(\mathbf{Q}) \implies \quad (122)$$

$$\frac{\|\mathbf{M}\|_F^2}{\text{Tr}(\mathbf{Q})} = \left(1 - \frac{\alpha_c}{\alpha} \right) \left(1 + \frac{\alpha_c^2}{\alpha} \sum_{(k,h) \in \mathcal{I}} c_{(k,h)}^2 \mathbb{E}_y[\lambda_k(y)^2 \lambda_h(y)] \right)^{-1} \quad (123)$$

As a special case, we consider the example $\lambda_k(y) = \lambda_h(y)$ for all h, k such that $\nu_{(k,k)} = \nu_{(h,h)} = \nu_1$. One instance for this case is given by the link function $g(\mathbf{z}) = p^{-1} \sum_{k \in \llbracket p \rrbracket} z_k^2$. Then, defining $\lambda^{(3)} = \mathbb{E}_y[\lambda_k(y)^3]$ for any $k | (k, k) \in \mathcal{I}$, the solution for m^2 does not depend on the coefficients $c_{(k,h)}$ and simplifies to

$$\frac{\|\mathbf{M}\|_F^2}{\text{Tr}(\mathbf{Q})} = \left(1 - \frac{\alpha_c}{\alpha} \right) \left(1 + \frac{\alpha_c^2}{\alpha} \lambda^{(3)} \right)^{-1}. \quad (124)$$

The above expression does not depend on the coefficients $c_{(k,h)}$, therefore it is valid for all the degenerate directions in the principal eigenspace.

We consider now specific cases of link functions that are such that $\text{Cov}[\mathbf{z}|y]$ is jointly diagonalizable $\forall y$. We refer to [Troiani et al. \[2024\]](#) for the derivation of the expressions of $Z(y)$ and $\text{Cov}[\mathbf{z}|y]$ in all the examples contained in this Appendix D.2.

³Note that $\forall k, h \in \llbracket p \rrbracket, \nu_{(k,h)} \leq \max(\nu_{(k,k)}, \nu_{(h,h)})$.

⁴Without loss of generality $\nu_{(h,h)} \leq \nu_{(k,k)}$ and $\nu_{(k,k)} = \nu_{(h,h)} \leq \sqrt{\nu_{(k,k)}\nu_{(h,h)}} \implies \nu_{(k,k)} \leq \nu_{(h,h)}$. Therefore $\nu_{(k,k)} = \nu_{(h,h)}$.

D.2.1 $g(z_1, \dots, z_p) = p^{-1} \sum_{k \in \llbracket p \rrbracket} z_k^2$

$$Z(y) = \frac{e^{-\frac{py}{2}}}{y^{2p/2} \Gamma\left(\frac{p}{2}\right)} (py)^{p/2}, \quad \text{Cov}[\mathbf{z}|y] = y \mathbf{I}. \quad (125)$$

For a generic $\mathbf{M} \in \mathbb{R}^{p \times p}$

$$\mathcal{F}(\mathbf{M}) = \mathbf{M} \int_0^\infty Z(y)(y-1)^2 dy = \frac{2}{p} \mathbf{M}, \quad (126)$$

$$\mathcal{G}(\mathbf{M}) = \mathbf{M} \mathbf{M}^T \int_0^\infty Z(y)(y-1)^3 dy = \frac{8}{p^2} \mathbf{M} \mathbf{M}^T, \quad (127)$$

therefore $\alpha_c = p/2$ and $\lambda^{(3)} = 8/p^3$. Plugging these quantities in eq. (124), the overlap matrices at convergence satisfy

$$\frac{\|\mathbf{M}\|_F^2}{\text{Tr}(\mathbf{Q})} = \begin{cases} \frac{1}{2}(2\alpha - p)(\alpha + 2)^{-1} & \alpha \geq p/2 \\ 0 & \alpha < p/2 \end{cases} \quad (128)$$

D.2.2 $g(z_1, z_2) = \text{sign}(z_1 z_2)$

$$Z(y) = \frac{1}{2}, \quad \text{Cov}[\mathbf{z}|y] = \frac{2y}{\pi} \begin{pmatrix} 0 & 1 \\ 1 & 0 \end{pmatrix} + \mathbf{I}. \quad (129)$$

The matrix $(\text{Cov}[\mathbf{z}|y] - \mathbf{I})$ is jointly diagonalizable $\forall y$, with eigenvalues $\lambda_1(y) = 2y\pi^{-1}$ and $\lambda_2(y) = -2y\pi^{-1}$. Therefore, the eigenvalues of \mathcal{F} are given by

$$\alpha_c^{-1} = \nu_{(1,1)} = \nu_{(2,2)} = \frac{4}{\pi^2}, \quad \nu_{(1,2)} = -\frac{4}{\pi^2}, \quad (130)$$

and

$$\mathbb{E}_y[\lambda_1(y)^3] = -\mathbb{E}_y[\lambda_2(y)^3] = \frac{8}{\pi^3} \sum_{y=\pm 1} y^3 = 0. \quad (131)$$

Leveraging eq. (123), the overlap matrices \mathbf{M} and \mathbf{Q} at convergence satisfy

$$\frac{\|\mathbf{M}\|_F^2}{\text{Tr}(\mathbf{Q})} = \begin{cases} 1 - \frac{\pi^2}{4} \alpha^{-1}, & \alpha \geq \pi^2/4 \\ 0, & \alpha < \pi^2/4 \end{cases} \quad (132)$$

D.2.3 $g(z_1, \dots, z_p) = \prod_{k=1}^p z_k$

For $p = 2$

$$Z(y) = \frac{K_0(|y|)}{\pi}, \quad \text{Cov}[\mathbf{z}|y] = \begin{pmatrix} |y|^{\frac{K_1(|y|)}{K_0(|y|)}} & y \\ y & |y|^{\frac{K_1(|y|)}{K_0(|y|)}} \end{pmatrix}, \quad (133)$$

where $K_n(y)$ is the modified Bessel function of the second kind. The matrix $\mathbf{G}(y)$ is jointly diagonalizable for all y , with eigenvalues $\lambda_1(y) = |y|^{\frac{K_1(|y|)}{K_0(|y|)}} + y - 1$ and $\lambda_2(y) = |y|^{\frac{K_1(|y|)}{K_0(|y|)}} - y - 1$. Therefore, the eigenvalues of \mathcal{F} are given by⁵

$$\alpha_c^{-1} = \nu_{(1,1)} = \nu_{(2,2)} = \mathbb{E}_y[\lambda_1(y)^2], \quad \nu_{(1,2)} = \mathbb{E}_y[\lambda_1(y)\lambda_1(-y)] < \nu_{(1,1)}, \quad (134)$$

⁵In what follows, we use $\lambda_1(y) = \lambda_2(-y)$, the parity of $Z(y)$ and the symmetry of the integration domain.

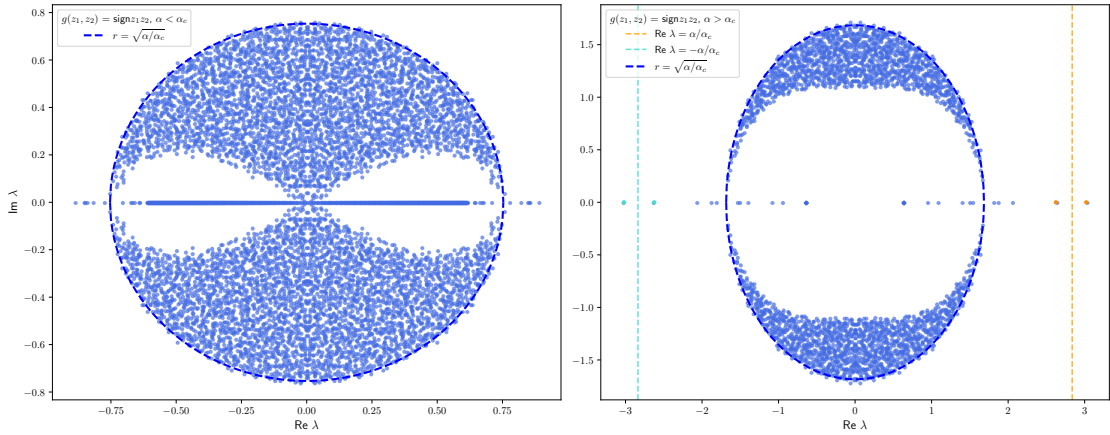


Figure 5: Distribution of the eigenvalues (dots) $\lambda \in \mathbb{C}$ of $\underline{\mathbf{L}}$ at finite $n = 5 \cdot 10^3$, for $g(z_1, z_2) = \text{sign}(z_1 z_2)$, $\alpha_c = \pi^2/4$. **(Left)** $\alpha = 1.4 < \alpha_c$. **(Right)** $\alpha = 7 > \alpha_c$. The dashed blue circle has radius equal to $\sqrt{\alpha/\alpha_c}$, i.e. the value γ_b predicted in Lemma 3.4. The dashed orange vertical line corresponds to $\text{Re } \lambda = \alpha/\alpha_c$, the eigenvalue γ_s defined in Lemma 3.3. As predicted by the state evolution equations for this problem, two significant eigenvalues (highlighted in orange) are observed near this vertical line. Additionally, one can observe that our framework predicts other two degenerate eigenvalues at $-\gamma_s$, here highlighted in cyan.

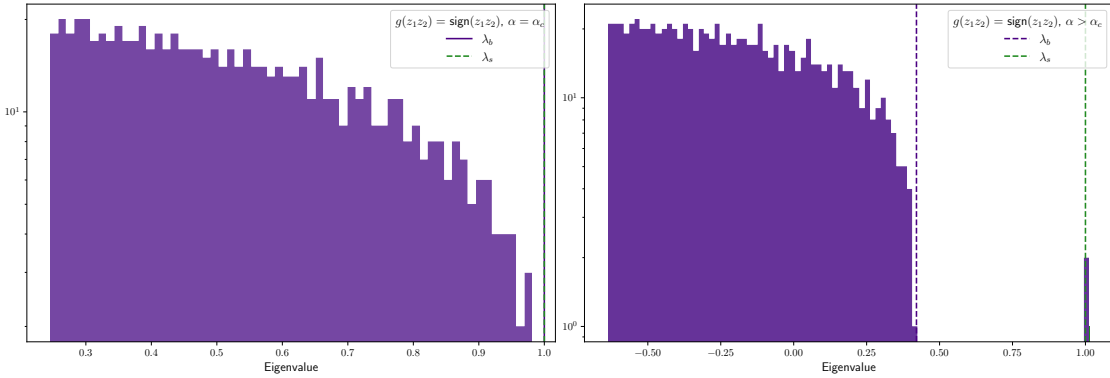


Figure 6: Distribution of the eigenvalues of $\underline{\mathbf{T}}$, $d = 10^4$, for the link function $g(z_1, z_2) = \text{sign}(z_1 z_2)$. The critical threshold in $\alpha_c = \pi^2/4$. The distribution is truncated on the left. **(Left)** $\alpha = \alpha_c$. **(Right)** $\alpha = 7 > \alpha_c$. As predicted by the state evolution framework, in this regime we observe two eigenvalues separated from the main bulk, centered around λ_s (green vertical line) obtained in Lemma 3.8. The vertical purple line correspond to the value λ_b provided in Lemma 3.9 as a bound for the bulk.

and

$$\mathbb{E}_y[\lambda_1(y)^3] = \mathbb{E}_y[\lambda_2(y)^3]. \quad (135)$$

Leveraging eq. (123), the overlap matrices \mathbf{M} and \mathbf{Q} at convergence satisfy

$$\frac{\|\mathbf{M}\|_{\text{F}}^2}{\text{Tr}(\mathbf{Q})} = \begin{cases} (\alpha - \alpha_c) (\alpha + \alpha_c^2 \mathbb{E}_{y \sim \mathbf{Z}} [\lambda_1(y)^3])^{-1}, & \alpha \geq \alpha_c \\ 0, & \alpha < \alpha_c \end{cases} \quad (136)$$

If instead $p \geq 3$,

$$\mathbf{Z}(y) = \frac{1}{(2\pi)^{p/2}} G_{0,p}^{p,0} \left(\frac{y^2}{2^p} \middle| \begin{array}{c} 0 \\ 0, 0, \dots, 0 \end{array} \right), \quad \text{Cov}[\mathbf{z}|y] = (\lambda(y) + 1) \mathbf{I}, \quad (137)$$

where

$$\lambda(y) = 2G_{0,p}^{p,0} \left(\frac{y^2}{2^p} \middle| \begin{array}{c} 0 \\ 0, 0, \dots, 0, 1 \end{array} \right) / G_{0,p}^{p,0} \left(\frac{y^2}{2^p} \middle| \begin{array}{c} 0 \\ 0, 0, \dots, 0 \end{array} \right) - 1, \quad (138)$$

and the previous expression are written in terms of the Meijer G -function. Therefore $\alpha_c^{-1} = \mathbb{E}_y[\lambda(y)^2]$ and, leveraging eq. (124), we obtain

$$\frac{\|\mathbf{M}\|_{\text{F}}^2}{\text{Tr}(\mathbf{Q})} = \begin{cases} (\alpha - \alpha_c) (\alpha + \alpha_c^2 \mathbb{E}_{y \sim \mathbf{Z}} [\lambda(y)^3])^{-1}, & \alpha \geq \alpha_c \\ 0, & \alpha < \alpha_c \end{cases} \quad (139)$$

D.3 A non-jointly diagonalizable case: $g(z_1, z_2) = z_1/z_2$

If the matrix $\mathbf{G}(y)$ is not jointly diagonalizable $\forall y$, there is not a general simplification for equations (75,76), and each example needs to be treated separately.

In this section we consider the Gaussian multi-index model with link function $g(z_1, z_2) = z_1/z_2$.

$$\mathbf{Z}(y) = \frac{1}{2\pi} \int_{\mathbb{R}^2} e^{-1/2(z_1^2 + z_2^2)} \delta \left(y - \frac{z_1}{z_2} \right) dz_1 dz_2 \quad (140)$$

$$= \frac{1}{2\pi} \int_{\mathbb{R}^2} |z_2| e^{-1/2(s^2 z_2^2 + z_2^2)} \delta(y - s) ds dz_2 \quad (141)$$

$$= \frac{1}{2\pi} \int_{\mathbb{R}} |z| e^{-1/2(y^2 + 1)z^2} dz = \frac{1}{\pi(y^2 + 1)} \quad (142)$$

In order to verify that both directions are not *trivial*, we need to compute $\mathbb{E}[\mathbf{z}|y]$ and verify that is zero almost surely over $y \sim \mathbf{Z}$:

$$\mathbb{E}_{\mathbf{z}}[\mathbf{z}|y] \propto \int_{\mathbb{R}^2} \mathbf{z} e^{-1/2(z_1^2 + z_2^2)} \delta \left(y - \frac{z_1}{z_2} \right) dz_1 dz_2 \quad (143)$$

$$= \int_{\mathbb{R}} \begin{pmatrix} yz \\ z \end{pmatrix} |z| e^{-1/2(y^2 + 1)z^2} dz = \mathbf{0}, \quad (144)$$

where the last equality is the result of the integral of an odd function over a symmetric domain. In order to study the performance of the spectral method, we compute

$$\text{Cov}[\mathbf{z}|y] = \frac{1}{2\pi \mathbf{Z}(y)} \int_{\mathbb{R}^2} \mathbf{z} \mathbf{z}^T e^{-1/2(z_1^2 + z_2^2)} \delta \left(y - \frac{z_1}{z_2} \right) dz_1 dz_2 \quad (145)$$

$$= \frac{1}{2\pi \mathbf{Z}(y)} \begin{pmatrix} y^2 & y \\ y & 1 \end{pmatrix} \int_{\mathbb{R}} |z|^3 e^{-1/2(y^2 + 1)z^2} dz \quad (146)$$

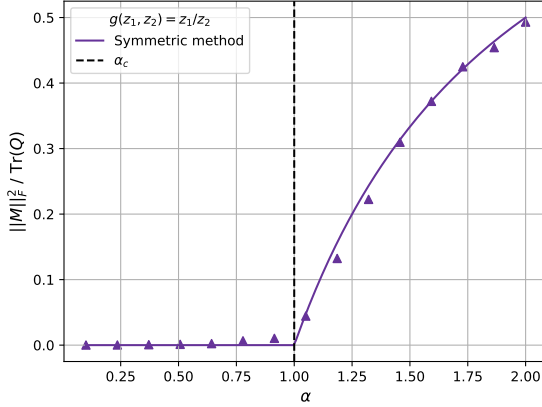


Figure 7: Overlap $\|\mathbf{M}\|_F^2 / \text{Tr}(\mathbf{Q})$ as a function of the sample complexity α . The dots represent numerical simulation results, computed for $n = 5000$ (for the asymmetric method) or $d = 5000$ (for the symmetric method) and averaging over 10 instances. The link function is $g(z_1, z_2) = z_1/z_2$. Solid lines are obtained from state evolution predictions. Dashed vertical line at $\alpha_c = 1$.

$$= \frac{1}{1+y^2} \begin{pmatrix} y^2-1 & 2y \\ 2y & 1-y^2 \end{pmatrix} + \mathbf{I}. \quad (147)$$

The eigenpairs of $(\text{Cov}[\mathbf{z}|y] - \mathbf{I})$ are $\lambda_1(y) = 1$, with eigenvector $(y, 1)^T$, and $\lambda_2(y) = -1$ with eigenvector $(-1, y)^T$, which depends on y . Considering a generic $\mathbf{M} = \begin{pmatrix} m_1 & m_2 \\ m_3 & m_4 \end{pmatrix}$, we have that

$$\mathcal{F}(\mathbf{M}) = \frac{\text{Tr}(\mathbf{M})}{2} \mathbf{I} + \frac{m_2 - m_3}{2} \begin{pmatrix} 0 & -1 \\ 1 & 0 \end{pmatrix}, \quad (148)$$

therefore, the eigenpairs of \mathcal{F} are

$$\nu_1 = 1, \mathbf{M}_1 = \mathbf{I}; \quad \nu_2 = 0, \mathbf{M}_2 = \begin{pmatrix} 1 & 0 \\ 0 & -1 \end{pmatrix}; \quad (149)$$

$$\nu_3 = 0, \mathbf{M}_3 = \begin{pmatrix} 0 & 1 \\ 1 & 0 \end{pmatrix}; \quad \nu_4 = -1, \mathbf{M}_4 = \begin{pmatrix} 0 & -1 \\ 1 & 0 \end{pmatrix}, \quad (150)$$

and $\alpha_c = 1$. Moreover, one could easily verify that $\mathcal{G}(\mathbf{M}_1) = \mathbf{0}$. The overlap of the spectral estimator with the signal is therefore $\mathbf{M} \propto \mathbf{I}$, and, from the state evolution eq. (76) at convergence, we have that

$$\frac{\|\mathbf{M}\|_F^2}{\text{Tr}(\mathbf{Q})} = \begin{cases} 1 - \alpha^{-1}, & \alpha \geq 1 \\ 0, & \alpha < 1 \end{cases} \quad (151)$$

where we leverage the symmetry of \mathbf{Q} in eq. (148) to write $\mathcal{F}(\mathbf{Q}) = 2^{-1} \text{Tr}(\mathbf{Q}) \mathbf{I} \implies \text{Tr}(\mathcal{F}(\mathbf{Q})) = \text{Tr}(\mathbf{Q})$.

E Details on examples - Symmetric spectral method

In all the considered examples with $p \geq 2$, the matrix $\text{Cov}[\mathbf{z}|y]$ admits a unique orthonormal basis of eigenvectors independent of y . Therefore, the state evolution equations can be significantly simplified

following the same considerations applied in Appendix D.2, to which we refer for the notation adopted in this appendix. Additionally, for all these examples, the eigenvalues $\lambda_k(y)$ of $(\text{Cov}[\mathbf{z}|y] - \mathbf{I})$ satisfy the additional conditions

$$\forall k, h \in \llbracket p \rrbracket, \quad \lambda_k(y) = \lambda_h(y) \text{ or } \begin{cases} \lambda_k(y) = \lambda_h(-y), \\ \mathbf{Z}(y) \text{ even and defined on a symmetric domain} \end{cases} \quad (152)$$

Additionally

$$\forall k, h \in \llbracket p \rrbracket, \quad \mathbb{E}_y[\lambda_k(y)\lambda_h(y)] \geq \mathbb{E}_y[\lambda_k(y)^2] = \mathbb{E}_y[\lambda_h(y)^2]. \quad (153)$$

It is easy to verify that these conditions implies that $\mathbf{V} = \mathbf{I}$, and the state evolution admits stable fixed point $\mathbf{M}, \mathbf{Q} \propto \mathbf{I}$, where the proportionality constants can be numerically computed through one-dimensional integrals, expressed in terms of $\lambda_1(y)$ (the choice of the eigenvalue is arbitrary in this setting) and given in eq. (54).

F Proof of Proposition 3.11

1. By definition $\underline{\mathbf{L}} \cdot \Omega = \gamma_{\underline{\mathbf{L}}}\Omega$. Applying on the right of both sides $\mathbf{X}^T \underline{\mathbf{G}} \cdot ((\gamma_{\underline{\mathbf{L}}}\mathbf{I} + \underline{\mathbf{G}})^{-1} \cdot \cdot)$

$$\mathbf{X}^T \underline{\mathbf{G}} \cdot ((\gamma_{\underline{\mathbf{L}}}\mathbf{I} + \underline{\mathbf{G}})^{-1} \cdot (\underline{\mathbf{L}} \cdot \Omega)) = \gamma_{\underline{\mathbf{L}}}\mathbf{X}^T \underline{\mathbf{G}} \cdot ((\gamma_{\underline{\mathbf{L}}}\mathbf{I} + \underline{\mathbf{G}})^{-1} \cdot \Omega). \quad (154)$$

Recalling the definition of $\underline{\mathbf{L}}$ (16)

$$\mathbf{X}^T \underline{\mathbf{G}} \cdot ((\mathbf{I} + \underline{\mathbf{G}})^{-1} \cdot (\mathbf{X}\mathbf{X}^T \underline{\mathbf{G}}\Omega)) = \mathbf{X}^T \underline{\mathbf{G}}\Omega \quad (155)$$

$$\implies \mathbf{X}^T \underline{\mathbf{G}} \cdot ((\underline{\mathbf{G}} + \gamma_{\underline{\mathbf{L}}}\mathbf{I})^{-1} \cdot (\mathbf{X}\mathbf{W})) = \mathbf{W} \quad (156)$$

2. Defining $\Omega := (\mathbf{I} + \underline{\mathbf{G}})^{-1} \cdot (\mathbf{X}\mathbf{W})$, we have that

$$\underline{\mathbf{L}} \cdot \Omega = (\mathbf{X}\mathbf{X}^T - \mathbb{I}_n)\underline{\mathbf{G}} \cdot ((\mathbf{I} + \underline{\mathbf{G}}^{-1} \cdot (\mathbf{X}\mathbf{W}))) \quad (157)$$

$$= \mathbf{X}\underline{\mathbf{T}} \cdot \mathbf{W} - \underline{\mathbf{G}}\Omega \quad (158)$$

$$= \gamma_{\underline{\mathbf{T}}}(\mathbf{I} + \underline{\mathbf{G}}) \cdot \Omega - \underline{\mathbf{G}} \cdot \Omega \quad (159)$$

$$= \gamma_{\underline{\mathbf{T}}}\Omega + (\gamma_{\underline{\mathbf{T}}} - 1)\underline{\mathbf{G}} \cdot \Omega. \quad (160)$$